AD NUMBER

ADB014423

LIMITATION CHANGES

TO:

Approved for public release; distribution is unlimited.

FROM:

Distribution authorized to U.S. Gov't. agencies only; Test and Evaluation; OCT 1976. Other requests shall be referred to Space and Missile Systems Organization, Los Angeles, CA 90009.

AUTHORITY

SAMSO ltr 19 Jan 1977

AEDC-TR-76-154

cy 2

EXPERIMENTAL RESULTS FROM A STATIC STABILITY AND PRESSURE TEST OF THE MINUTEMAN INSTRUMENTED PAYLOAD DELIVERY SYSTEM LAUNCH VEHICLE CONFIGURATION AT MACH NUMBERS FROM 1.6 TO 5.0

VON KÁRMÁN GAS DYNAMICS FACILITY
ARNOLD ENGINEERING DEVELOPMENT CENTER
AIR FORCE SYSTEMS COMMAND
ARNOLD AIR FORCE STATION, TENNESSEE 37389

October 1976

Final Report for Period April 21 – 29, 1976

This document has been approved for public release
its distribution is unlimited. per TAB 77-9 4/24/77

F40600-75-C-0002

Prepared for

SPACE AND MISSILE SYSTEMS ORGANIZATION (RSTB)
P. O. BOX 92960, WORLDWAY POSTAL CENTER
LOS ANGELES, CALIFORNIA 90009

NOTICES

When U. S. Government drawings specifications, or other data are used for any purpose other than a definitely related Government procurement operation, the Government thereby incurs no responsibility nor any obligation whatsoever, and the fact that the Government may have formulated, furnished, or in any way supplied the said drawings, specifications, or other data, is not to be regarded by implication or otherwise, or in any manner licensing the holder or any other person or corporation, or conveying any rights or permission to manufacture, use, or sell any patented invention that may in any way be related thereto.

Qualified users may obtain copies of this report from the Defense Documentation Center.

References to named commercial products in this report are not to be considered in any sense as an endorsement of the product by the United States Air Force or the Government.

APPROVAL STATEMENT

This technical report has been reviewed and is approved for publication.

FOR THE COMMANDER

Chauncey D. Smith, Jr.

CHAUNCEY D. SMITH, JR.
Lt Colonel, USAF
Chief Air Force Test Director, VKF
Directorate of Test

Alan L. Devereaux

ALAN L. DEVEREAUX
Colonel, USAF
Director of Test

REPORT DOCUMENTATION PAGE		READ INSTRUCTIONS BEFORE COMPLETING FORM
1 REPORT NUMBER AEDC-TR-76-154	2 GOVT ACCESSION NO.	3 RECIPIENT'S CATALOG NUMBER
4 TITLE (and Subtitle) EXPERIMENTAL RESULTS FROM A STATIC STABILITY AND PRESSURE TEST OF THE MINUTEMAN INSTRUMENTED PAYLOAD DELIVERY SYSTEM LAUNCH VEHICLE CONFIGURATION AT MACH NUMBERS FROM 1.6 TO 5.0		5 TYPE OF REPORT & PERIOD COVERED Final Report - April 21 - 29, 1976 6 PERFORMING ORG REPORT NUMBER
7 AUTHOR(s) E. E. Lindsay and D. H. Fikes, ARO, Inc.		8 CONTRACT OR GRANT NUMBER(s)
9 PERFORMING ORGANIZATION NAME AND ADDRESS Arnold Engineering Development Center (XO) Air Force Systems Command Arnold Air Force Station, Tennessee 37389		10 PROGRAM ELEMENT, PROJECT, TASK AREA & WORK UNIT NUMBERS Program Element 63311F System 627A; Task 01
11 CONTROLLING OFFICE NAME AND ADDRESS Space and Missile Systems Organization (RSTB), P.O. Box 92960, Worldway Postal Center, Los Angeles, California 90009		12 REPORT DATE October 1976 13 NUMBER OF PAGES 48
14 MONITORING AGENCY NAME & ADDRESS(if different from Controlling Office)		15 SECURITY CLASS. (of this report) UNCLASSIFIED 15a DECLASSIFICATION/DOWNGRADING SCHEDULE N/A

16 DISTRIBUTION STATEMENT (of this Report)
Distribution limited to U.S. Government agencies only; this report contains information on test and evaluation of military hardware; October 1976; other requests for this document must be referred to Space and Missile Systems Organization (RSTB), P.O. Box 92960, Worldway Postal Center, Los Angeles, California 90009.

17 DISTRIBUTION STATEMENT (of the abstract entered in Block 20, if different from Report)

18 SUPPLEMENTARY NOTES

Available in DDC

19 KEY WORDS (Continue on reverse side if necessary and identify by block number)

static force
pressure (surface)
Minuteman Instrumented Payload Delivery System (MIPDS)
Mach numbers
Reynolds numbers
angles
roll
angle of attack

20 ABSTRACT (Continue on reverse side if necessary and identify by block number)

Static-force and moment and surface pressure data were obtained on a 0.06-scale representation of the Minuteman Instrumented Payload Delivery System (MIPDS) launch vehicle. The test was conducted at Mach numbers from 1.6 to 5.0 at free-stream Reynolds numbers, based on model length, from 28.4 to 23.6 million, respectively. The angle-of-attack range was

DD FORM 1 JAN 73 1473 EDITION OF 1 NOV 65 IS OBSOLETE

20. ABSTRACT (Continued)

from -12 to 12 deg, and the roll angle range was from -180 to 180 deg. Results are presented to illustrate typical effects of variations in vehicle configuration, vehicle attitude, and Mach number on the static aerodynamic and surface pressure characteristics of the MIPDS payload nose section and the complete launch vehicle.

AFSC
Arnold AFS Tenn

PREFACE

The work reported herein was conducted by the Arnold Engineering Development Center (AEDC), Air Force Systems Command (AFSC), at the request of the Space and Missile Systems Organization (SAMSO), AFSC, Los Angeles, California, for TRW, Inc., Redondo Beach, California, under Program Element 63311F, System 627A, Task 01. The results were obtained by ARO, Inc. (a subsidiary of Sverdrup & Parcel and Associates, Inc.), contract operator of AEDC, AFSC, Arnold Air Force Station, Tennessee. The work was done under ARO Project No. V41A-G1A. The authors of this report were E. E. Lindsay and D. H. Fikes, ARO, Inc. The final data package was completed on June 22, 1976, and the manuscript (ARO Control No. ARO-VKF-TR-76-89) was submitted for publication on August 11, 1976.

The authors wish to acknowledge the work done by E. O. Marchand of the von Kármán Gas Dynamics Facility (VKF) in providing the theoretical calculations used in this report.

CONTENTS

ILLUSTRATIONS

TABLES

1.0 INTRODUCTION

An experimental force and pressure investigation was conducted in the von Kármán Gas Dynamics Facility (VKF) Supersonic Wind Tunnel (A) at Mach numbers from 1.6 to 5.0 on the Minuteman Instrumented Payload Delivery System (MIPDS) launch vehicle configuration. The test was performed to obtain static aerodynamic and surface pressure distribution data on the complete launch vehicle configuration and the newly designed payload nose section. The experimental results from the test will be used to verify the aerodynamic estimates used in the structural, controls, and trajectory analyses of the MIPDS launch vehicle by TRW.

Static stability and axial-force data were obtained on the complete launch vehicle and the payload nose section for variations in model attitude and Mach number. Effects of boundary-layer trips on total vehicle and payload nose section performance and the effects of booster raceway components and a seal at the nose section joint on the aerodynamic characteristics of the complete vehicle were investigated. The force test phase was conducted at Mach numbers 1.62, 2.00, 3.01, 3.51, 3.76, 4.02, and 5.06 and free-stream unit Reynolds numbers of 7.7, 8.1, 7.2, 6.2, 6.0, 5.9, and 6.4 million per foot, respectively. The angle-of-attack range was from approximately -6 to 12 deg, and the roll angle range was from -180 to 180 deg.

Surface pressure distribution data were obtained on the complete launch vehicle at Mach numbers 1.62, 2.00, 3.01, 4.02, and 5.06 at free-stream unit Reynolds numbers of 7.7, 8.1, 7.2, 5.9, and 6.4 million per foot, respectively. Effects of boundary-layer trip devices on the pressure distribution over the vehicle were also investigated at Mach numbers 1.62 and 4.03. The angle-of-attack range was from -12 and 12 deg, and the roll angle range was from -90 to 180 deg.

2.0 APPARATUS

2.1 WIND TUNNEL

Tunnel A (Fig. 1) is a continuous, closed-circuit, variable density wind tunnel with an automatically driven flexible-plate-type nozzle and a 40- by 40-in. test section. The tunnel can be operated at Mach numbers from 1.5 to 6 at maximum stagnation pressures from 29 to 200 psia, respectively, and stagnation temperatures up to 750°R (M_∞ = 6). Minimum operating pressures range from about one-tenth to one-twentieth of the maximum at each Mach number. The tunnel is equipped with a model injection system which allows removal of the model from the test section while the tunnel remains in operation. A description of the tunnel and airflow calibration information may be found in Ref. 1.

2.2 MODEL

Photographs and details of the 0.06-scale model of the Minuteman Instrumented Payload Delivery System launch vehicle are shown in Figs. 2 and 3. The model was designed and fabricated by Ellco Engineering, Inc., for TRW and SAMSO (RSTB). The MIPDS launch vehicle configuration consisted of a newly designed payload nose section, a booster section, and four nozzles attached to the booster afterbody; the model, including the nozzles, was 44.268 in. long. The nose section extended to model station (MS) 15.445, and the downstream booster section had an afterbody diameter of 3.942 in. The model was designed so that all hardware components, except the nose section, could be used with either the force or pressure model.

The force model utilized two six-component balances to provide for the simultaneous acquisition of the aerodynamic loads on the total vehicle and the payload nose section. The simultaneous measurement of total vehicle and nose section loads was made with no seal at the metric break (MS 15.445), which provided a 0.023-in. interference-free gap between the nose and booster sections. The base cavity of the nose section at the gap was also vented into the booster section cavity to reduce any effects of flow across the gap on total vehicle and nose section measurements. A solid seal which hard-mounted the payload nose to the booster section and a removable booster raceway were also provided.

The pressure model was instrumented with 95 pressure orifices with 51 located in the payload nose section and 44 in the booster section. The pressure orifices in the booster section, which was common to both the force and pressure model, were sealed off during the force test phase. The pressure model used the solid seal to hard-mount the nose section to the booster section without the raceway to provide the only configuration run during the pressure test phase. The locations of the pressure orifices are listed in Table 1.

Trip geometries were the same for both test phases and are shown in Fig. 3b. A description of the model components employed during the test is given in the Nomenclature.

2.3 INSTRUMENTATION AND PRECISION

Tunnel A stilling chamber pressure is measured with a 15-, 60-, 150-, or 300-psid transducer referenced to a near vacuum. Based on periodic comparisons with secondary standards, the uncertainty (a bandwidth which includes 95 percent of the residuals) of these transducers is estimated to be within ±0.2 percent of reading or ±0.015 psia,

whichever is greater. Stilling chamber temperature is measured with a copper-constantan thermocouple with an uncertainty of ±3°F based on repeat calibrations.

Total vehicle and payload nose section forces and moments were measured with six-component, moment-type, strain-gage balances supplied and calibrated by VKF. Prior to the test, static loads in each plane and combined static loads were applied to the balances to simulate the range of loads and center-of-pressure locations anticipated during the test. The following uncertainties represent the bands of 95 percent of the measured residuals, based on differences between the applied loads and the corresponding values calculated from the balance calibration equations included in the final data reduction. The range of check loads applied and the measurement uncertainties follow.

Total Vehicle Balance

Component	Balance Design Loads	Calibration Load Range	Range of Check Loads	Measurement Uncertainty
Normal force, lb	±500	±250	±100	±0.8
Pitching Moment*, in.-lb	±1,850	±925	±625	±2.2
Side Force, lb	±250	±250	±100	±1.2
Yawing Moment*, in.-lb	±925	±925	±625	±2.0
Rolling Moment, in.-lb	±100	±35	-	±0.3
Axial Force, lb	±300	0-100	-	±0.2

*About balance forward moment bridge

The transfer distance from the balance forward moment bridge to the booster moment reference location was 11.393 in. along the longitudinal axis and was measured with an estimated precision of ±0.005 in.

Payload Nose Section Balance

Component	Balance Design Loads	Calibration Load Range	Range of Check Loads	Measurement Uncertainty
Normal Force, lb	±200	±100	±50	0.50
Pitching Moment*, in.-lb	±680	±340	±100	0.20
Side Force, lb	±200	±100	±50	0.10
Yawing Moment*, in.-lb	±680	±340	±100	0.35
Rolling Moment, in.-lb	±100	±25	-	0.10
Axial Force, lb	±50	0-30	-	0.09

*About balance forward moment bridge

The transfer distance from the balance forward moment bridge to the nose moment reference location was 2.316 in. along the longitudinal axis and was measured with an estimated precision of ±0.005 in.

Model surface, cavity, and base pressures were measured with the Tunnel A standard pressure system which uses 15-psid transducers referenced to a near vacuum or a variable reference and having full-scale calibrated ranges of 1, 5, and 15 psia. Based on periodic comparisons with secondary standards, the precision is estimated to be ±0.15 percent of the reading or ±0.003 psi, whichever is the larger.

Shadowgraphs or schlierens were obtained on several configurations at selected attitudes and test conditions. The flow-field photographs were recorded with a double pass optical flow visualization system with a 35-in.-diam field of view.

3.0 PROCEDURE

3.1 TEST CONDITIONS

The test was conducted at Mach numbers from 1.62 to 5.06 at free-stream unit Reynolds number of 5.9 to 8.1 million per ft. A summary of the test conditions at each Mach number is given below.

Data*	M_∞	p_o, psia	T_o, °R	q_∞, psia	p_∞, psia	$Re_\infty \times 10^{-6}$
F,P	1.62	28.0	570	11.74	6.39	7.7
F,P	2.00	34.0	570	12.16	4.34	8.1
F,P	3.01	50.0	570	8.52	1.34	7.2
F	3.51	56.0	570	6.24	0.72	6.2
F	3.76	64.0	580	5.78	0.58	6.0
F,P	4.02	72.0	580	5.22	0.46	5.9
F,P	5.06	150.0	635	4.74	0.26	6.4

*F - Force data; P - Pressure data

Test summaries showing all configurations tested and the variables for each are presented in Tables 2 and 3 for the force and pressure test phases, respectively.

3.2 TEST PROCEDURE

3.2.1 General

In Tunnel A, the model is mounted on a sting support mechanism located in an installation tank directly underneath the tunnel test area. The installation tank is separated from the tunnel by a pair of fairing doors and a safety door. When closed, the fairing doors, except for a slot for the pitch sector, cover the opening to the tank and the safety door seals the tunnel from the tank area. After the model is prepared for a data run, the personnel access door to the installation tank is closed, the tank is vented to the tunnel flow, and the safety and fairing doors are opened. Then the model is injected into the airstream and, after it reaches tunnel centerline, is translated forward into the test section. After the data run is completed, the model is returned into the tank and the fairing and safety doors are closed sealing the tank from the tunnel. The tank is then vented to atmosphere with the tunnel running to allow access to the model in preparation for the next run. The sequence is repeated after each configuration or test condition change.

Model attitude positioning and data recording were accomplished with either the pitch-pause or the continuous sweep mode of operation. The VKF-built Programmed Position Control System (PPCS) was modified for the test and was used during both the force and pressure phases to greatly increase the data acquisition rate. Model pitch and roll requirements were programmed into the PPCS before the test was begun. Model positioning and data recording operations were performed automatically during each test phase by selecting the desired attitude matrix and mode of operation and initiating the PPCS.

3.2.2 Force Phase

The force phase was performed in both the pitch-pause and continuous sweep modes of operation. The pitch-pause method was used during angle-of-attack variations at constant roll angles to obtain base and cavity pressure measurements simultaneously with the force measurements. At each model attitude in this mode, the control system delayed the data acquisition sequence until the base and cavity pressures stabilized. The continuous sweep technique was used to obtain force data as the roll angle varied from -180 to 180 deg at a constant angle of attack. Base and cavity pressures were not measured during the continuous sweep mode because of the relatively slow response time of the standard pressure measuring system. Data were sampled at a rate of 900 channels/sec, and 14 data loops were averaged for each data point.

3.2.3 Pressure Phase

The pressure phase was performed in the pitch-pause mode of operation. Model pressure measurements were obtained at discrete attitudes as the roll angle was varied in increments from -90 to 180 deg at a constant angle of attack. After the model reached each position in the roll-pitch matrix, the pressures were allowed to stabilize before one complete scan of the data was recorded and the model was driven to the next position. Data acquisition and model positioning were performed automatically after the test sequence was initiated.

3.3 DATA REDUCTION

3.3.1 Static-Force Data

Force and moment measurements were reduced to coefficient form using the force and moment values calculated from the averaged data points and corrected for first- and second-order balance interaction effects. Total vehicle and payload nose section coefficients also were corrected for model tare weight and balance-sting deflections. Model attitude, base pressure, cavity pressure, and tunnel pressure and temperature were also calculated from averaged values.

Total vehicle and payload nose section aerodynamic coefficients are presented in the nonrolled missile axis system; that is, the normal-force direction is always in the pitch plane of the tunnel and normal to the longitudinal axis of the model. Vehicle pitching- and yawing-moment coefficients are referenced to MS 34.074, and nose section pitching- and yawing-moment coefficients are referenced to MS 10.525. Booster afterbody diameter (3.942 in.) and area (12.205 in.^{2}) were used as the reference length, d, and area, S, for both vehicle and nose section aerodynamic coefficients. Total vehicle and payload nose section forebody axial-force coefficients (C_A and C_{A_N}) have been adjusted to zero base axial force using measured vehicle and nose section cavity and base pressures. Vehicle and nose attitudes have been corrected for model misalignment and flow angularity.

3.3.2 Pressure Data

Model surface pressure data were obtained using the Tunnel A standard pressure system. The measured pressure was reduced to coefficient form using values for tunnel free-stream static and dynamic pressures which were calculated using the measured tunnel stilling chamber pressure and the test section Mach number determined from tunnel flow calibrations. Model angle of attack was corrected for sting deflection using the model

loads obtained during the force phase and the deflection constants for the pressure model sting arrangement. Model angle of attack was also adjusted for flow angularity.

3.4 DATA UNCERTAINTY

An evaluation of the influence of random measurement errors is presented in this section to provide a partial measure of the uncertainty of the final test results presented in this report. Although evaluation of the systematic measurement error (bias) is not included, it should be noted that the instrumentation precision values (give in Section 2.3) used in this evaluation represent a total uncertainty combination of both systematic and two-sigma random error contributions.

3.4.1 Test Conditions

Uncertainties in the basic tunnel parameters p_o and T_o (see Section 2.3) and the two-sigma deviation in Mach number determined from test section flow calibrations were used to estimate uncertainties in the other free-stream properties, using the Taylor series method of error propagation.

	Uncertainty (±), percent					
M_∞	M_∞	p_o	T_o	p_∞	q_∞	Re_∞
1.62	1.1	0.2	0.5	3.0	0.8	1.0
2.00	1.0	↓	↓	3.0	1.1	1.1
3.01	0.7	↓	↓	3.0	1.7	1.3
3.51	0.5	↓	↓	2.8	1.7	1.3
3.76	0.5	↓	↓	2.8	1.7	1.3
4.02	0.5	↓	↓	2.7	1.7	1.3
5.06	0.3	↓	↓	1.7	1.2	1.1

3.4.2 Static-Force Data

The balance and pressure uncertainties listed in Section 2.3 were combined with uncertainties in the tunnel parameters, using the Taylor series method of error propagation, to estimate the uncertainty of the aerodynamic coefficients, and these are presented on the following page.

Uncertainty (±)

Maximum Measured Coefficient Value, percent

Total Vehicle Coefficients

M_∞	C_N	C_m	C_Y	C_n	C_ℓ	C_A
1.62	0.9	1.0	1.0	1.2	1.8	1.1
2.00	1.2	1.3	1.4	1.5	2.0	1.8
3.01	1.8	1.9	1.9	2.2	3.2	2.5
3.51	1.8	2.1	2.0	2.5	4.1	2.7
3.76	1.7	1.7	1.7	1.7	3.5	2.2
4.02	1.9	2.5	2.3	3.1	3.7	3.1
5.06	1.7	2.4	2.1	3.2	4.0	2.7

Payload Nose Section Coefficients

M_∞	C_{N_N}	C_{m_N}	C_{Y_N}	C_{n_N}	C_{ℓ_N}	C_{A_N}
1.62	0.8	0.9	0.6	0.9	*	1.2
2.00	1.2	1.4	1.1	1.5	↓	1.7
3.01	1.7	2.2	1.7	2.3	↓	2.9
3.50	1.7	2.4	1.6	2.6	↓	3.0
4.02	1.9	2.8	1.8	3.3	↓	3.3
5.06	1.7	2.4	1.3	2.9	↓	2.7

*These uncertainties are not presented because the maximum measured coefficients were only a few times more than the values of the repeatabilities shown on the following page.

The basic precision of the aerodynamic coefficients was also computed using only the balance and pressure uncertainties listed in Section 2.3 along with the nominal test conditions, using the assumption that the free-stream flow nonuniformity is a bias type of uncertainty which is constant for all test runs. These values, therefore, represent the data repeatability expected and are especially useful for detailed discrimination purposes in parametric model studies.

Repeatability (±), Measured Coefficient Value

Total Vehicle Coefficients

M_∞	C_N	C_m	C_Y	C_n	C_ℓ	C_A
1.62	0.0056	0.0039	0.0084	0.0035	0.0005	0.0014
2.00	0.0053	0.0038	0.0081	0.0034	0.0005	0.0013
3.01	0.0077	0.0054	0.0115	0.0049	0.0007	0.0019
3.51	0.0105	0.0073	0.0158	0.0067	0.0010	0.0026
3.76	0.0113	0.0079	0.0170	0.0072	0.0011	0.0028
4.02	0.0126	0.0088	0.0188	0.0080	0.0012	0.0031
5.06	0.0138	0.0096	0.0207	0.0088	0.0013	0.0035

Payload Nose Section Coefficients

M_∞	C_{N_N}	C_{m_N}	C_{Y_N}	C_{n_N}	C_{ℓ_N}	C_{A_N}
1.62	0.0010	0.0004	0.0007	0.0006	0.0002	0.0006
2.00	0.0010	0.0003	0.0007	0.0006	0.0002	0.0006
3.01	0.0014	0.0005	0.0010	0.0009	0.0002	0.0009
3.05	0.0020	0.0007	0.0013	0.0012	0.0003	0.0012
4.02	0.0024	0.0008	0.0016	0.0014	0.0004	0.0014
5.06	0.0026	0.0009	0.0017	0.0015	0.0004	0.0016

3.4.3 Pressure Data

The precision of the model pressure coefficients was estimated using the instrumentation precisions quoted in Section 2.3 and the uncertainties in the free-stream flow conditions combined with the Taylor series error propagation method. Uncertainties in the pressure coefficients are as follows:

Maximum Uncertainty

M_∞	CP
1.62	0.006
2.00	0.004
3.00	0.004
4.02	0.004
5.06	0.004

3.4.4 Model Attitude

The uncertainty in vehicle (α and ϕ) and nose section attitude (α_N and ϕ_N), as determined from tunnel sector calibrations and consideration of the possible errors in model deflection and flow angularity calculations, is estimated to be ±0.10 deg.

4.0 RESULTS AND DISCUSSION

The purpose of the test program was to obtain experimental static-force and surface pressure data on the Minuteman Instrumented Payload Delivery System launch vehicle configuration at Mach numbers from 1.62 to 5.06. Results from the test have been transmitted to the test contractor (TRW) and the sponsor (SAMSO/RSTB), and the contractor will provide the sponsor with a complete analysis of the force and pressure data. Therefore, the purpose of this report is to document the test and present selected test results to illustrate typical effects of the primary variables investigated.

Typical static-force results for the total vehicle and payload nose section are shown in Figs. 4 thru 11. The aerodynamic coefficients are presented for the nonrolled missile axis system. Total vehicle pitching- and yawing-moment coefficients are referenced to MS 34.074 and payload nose section pitching- and yawing-moment coefficients to MS 10.525. Any reference to vehicle or nose static stability characteristics in subsequent discussions will apply only to the vehicle and nose section with these moment reference locations. Total vehicle and payload nose section forebody axial-force coefficients have been adjusted to zero base axial force using measured base and cavity pressures. The longitudinal stability and axial-force characteristics are presented as functions of angle of attack and side-force, yawing-moment, and rolling-moment characteristics as functions of roll attitude.

Figures 4 and 5 illustrate typical effects of Mach number variation on total vehicle and payload nose section aerodynamic characteristics. Figure 4 shows the strong sensitivity of vehicle and nose section axial-force measurements to variations in Mach number as the axial-force coefficient values decreased approximately 50 percent as Mach number increased from 1.62 to 5.06. The vehicle and nose section configurations were longitudinally unstable at all Mach numbers, and Fig. 4 shows that there was little effect of Mach number variations on the stability characteristics of these configurations above Mach number 3.01. The cyclic trends of the vehicle and nose section yaw plane measurements presented in Fig. 5 represent the influence of the model asymmetry as the model was rolled from -180 to 180 deg. The general characteristics of the vehicle and nose side-force and rolling-moment measurements were essentially independent of Mach number. However, Fig. 5 indicates an apparent Mach number sensitive crossflow effect on

vehicle yawing-moment measurements when the raceway was to the lee side (ϕ = 90 to 180 deg). A trend reversal for nose yawing-moment measurements between Mach number 2.00 and 3.01 is also noted.

The small influence of boundary-layer trip geometry on the aerodynamic characteristics of the total vehicle and payload nose section is shown in Figs. 6 and 7 for Mach number 4.02. An increase in the nose axial-force coefficient of approximately eight percent near zero angle of attack was the most evident effect noted when a second trip was added downstream of the baseline trip T2 (see Fig. 3b).

Typical effects of variation in model attitude on total vehicle and payload nose section aerodynamic characteristics are illustrated in Figs. 8 and 9 for Mach number 3.01. Figure 8 indicates that variations in roll attitude produced relatively small responses in vehicle and nose pitch plane measurements. The strong influence of angle-of-attack variation on vehicle side-force, yawing-moment, and rolling-moment coefficients is shown in Fig. 9a with the magnitude of the coefficient values increasing significantly with increasing angle of attack. Although the trend of the nose measurements shown in Fig. 9b was similar to the vehicle measurements, the relative magnitude of the nose coefficients changes was much less for variations in angle of attack. Vehicle and nose section peak measurement roll locations were rather insensitive to variations in angle of attack.

The effect of the booster raceway on the total vehicle aerodynamic characteristics is shown in Fig. 10 for Mach number 3.01. Figure 10a indicates that the addition of the raceway to the booster section had little measurable effect on vehicle pitch plane characteristics except for a slight forward movement in the center of pressure at positive angles of attack. This small center-of-pressure shift was not unexpected because of the raceway geometry and location (see Fig. 3a). Figure 10b indicates the sensitivity of the vehicle yaw plane coefficients to the addition of the raceway to the model. As the model rolled from -180 to 180 deg, the raceway produced relatively large variations in all yaw plane measurements.

The good agreement of the total vehicle aerodynamic data obtained with an open gap (S1) and a solid metal-to-metal seal (S3) between the nose and booster sections is illustrated in Fig. 11 for Mach number 3.01. These results show that the use of the open gap to permit the simultaneous recording of payload nose and total vehicle force and moment measurements did not unduly compromise data quality, particularly in the pitch plane, while doubling the data acquisition rate.

Typical surface pressure results are presented in coefficient form in Figs. 12 through 15. Longitudinal pressure distributions along the vehicle are shown for the most instrumented ray (θ = 90 deg). The experimental results are also compared to theoretical calculations for Mach numbers 2.00, 3.01, 4.02, and 5.06 at α = 0 and for α = 0, 4, 8, and 12 deg at Mach number 3.01.

The theoretical values presented were obtained using computer codes which are described in Refs. 2 thru 4 and which numerically solve the differential equations governing the flow of an inviscid fluid. The expansion and compression corners were approximated by polynomials to allow continuity of the body geometry. The code described in Ref. 2 is a time dependent technique and was used to obtain a solution over the subsonic portion of the spherical nose. A reference plane method, described in Ref. 3, was then used to take the body normal axisymmetric solution of the subsonic region and generate a three-dimensional axis-normal supersonic solution at the sphere-ogive tangent point. The shock capturing code described in Ref. 4 was then used to calculate the flow field over the remainder of the body.

Figure 12 illustrates the influence of Mach number variation on the longitudinal surface pressure distribution along the vehicle at zero angle of attack. The results show similar trends in the longitudinal distributions with different levels characteristic of each Mach number. Comparisons of the experimental longitudinal surface pressure distributions for Mach numbers of 2.00, 3.01, 4.02, and 5.06 with theoretical calculations in Figs. 12 thru 15 show relatively good agreement at each Mach number for this model geometry.

The small effect of boundary-layer trips on the longitudinal surface pressure distributions is presented in Fig. 13 for Mach number 4.02 and zero angle of attack. The addition of one (T2) or two (T3) trip devices to the clean configuration produced only small variations in the pressure measurements in the regions of the two downstream compression surfaces on the booster section. Although not shown, radial surface pressure distributions for four model stations also showed little effect of trip geometry.

Longitudinal windward surface pressure distributions along the vehicle are shown in Fig. 14 for angles of attack of 0, 4, 8, and 12 deg at Mach number 3.01. The results shown are for the θ = 90-deg ray and with the model rolled 90 deg to position the instrumented ray to windward. These data illustrate the typical pressure level changes associated with angle-of-attack variations and show good agreement with the calculated theoretical values at each angle of attack.

The quality of the repeatability of the pressure measurements is illustrated in Fig. 15 for Mach number 3.01 and zero angle of attack. Longitudinal distributions are presented for model roll angles of -90, 0, and 90 deg and indicate that data repeatability

was very good. An evaluation of test results at the other Mach numbers also indicated a similar repeatability quality.

5.0 SUMMARY OF RESULTS

A static-force and pressure test was conducted on the Minuteman Instrumented Payload Delivery System launch configuration at Mach numbers from 1.62 to 5.06, at angles of attack from -12 to 12 deg, and roll angles from -180 to 180 deg. The test results are summarized as follows:

1. A dual-balance arrangement was successfully employed to simultaneously obtain static-force data on the total vehicle and the payload nose section.

2. An open gap (no seal) between the nose and booster sections had no significant influence on total vehicle static-force characteristics.

3. Variations in boundary-layer trip geometry produced only a small measurable effect on static-force and surface pressure results.

4. Experimental pressure data agreed satisfactorily with theoretical estimates.

REFERENCES

1. Test Facilities Handbook (Tenth Edition) "von Kármán Gas Dynamics Facility, Vol. 3." Arnold Engineering Development Center, May 1974.

2. Aungier, R. H. "A Computational Method for Exact, Direct, and Verified Solutions for Axisymmetric Flow over Blunt Bodies of Arbitrary Shape." AFWL-TR-70-16, July 1970.

3. Rakich, J. V. "A Method of Characteristics for Steady Three-Dimensional Supersonic Flow with Application to Inclined Bodies of Revolution." NASA TN D-5341, October 1969.

4. Kutler, P., Reinhardt, W. A., and Warming, R. F. "Numerical Computation of Multishocked, Three-Dimensional Supersonic Flow Fields with Real Gas Effects." AIAA Paper 72-702 Presented at the AIAA 5th Fluid and Plasma Dynamics Conference, Boston, Massachusetts, June 26-28, 1972.

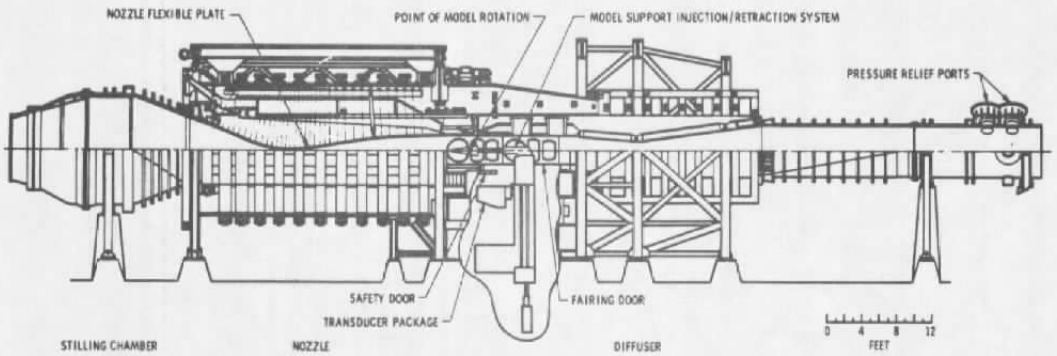

a. VKF Tunnel A

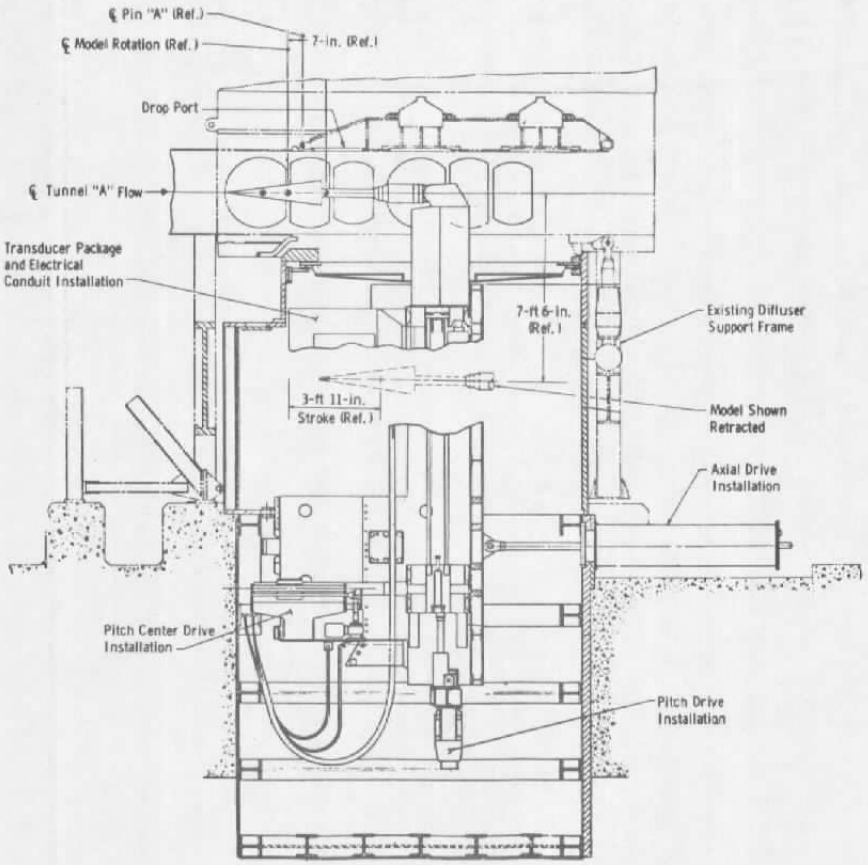

b. Model injection system

Figure 1. Wind tunnel and model injection system.

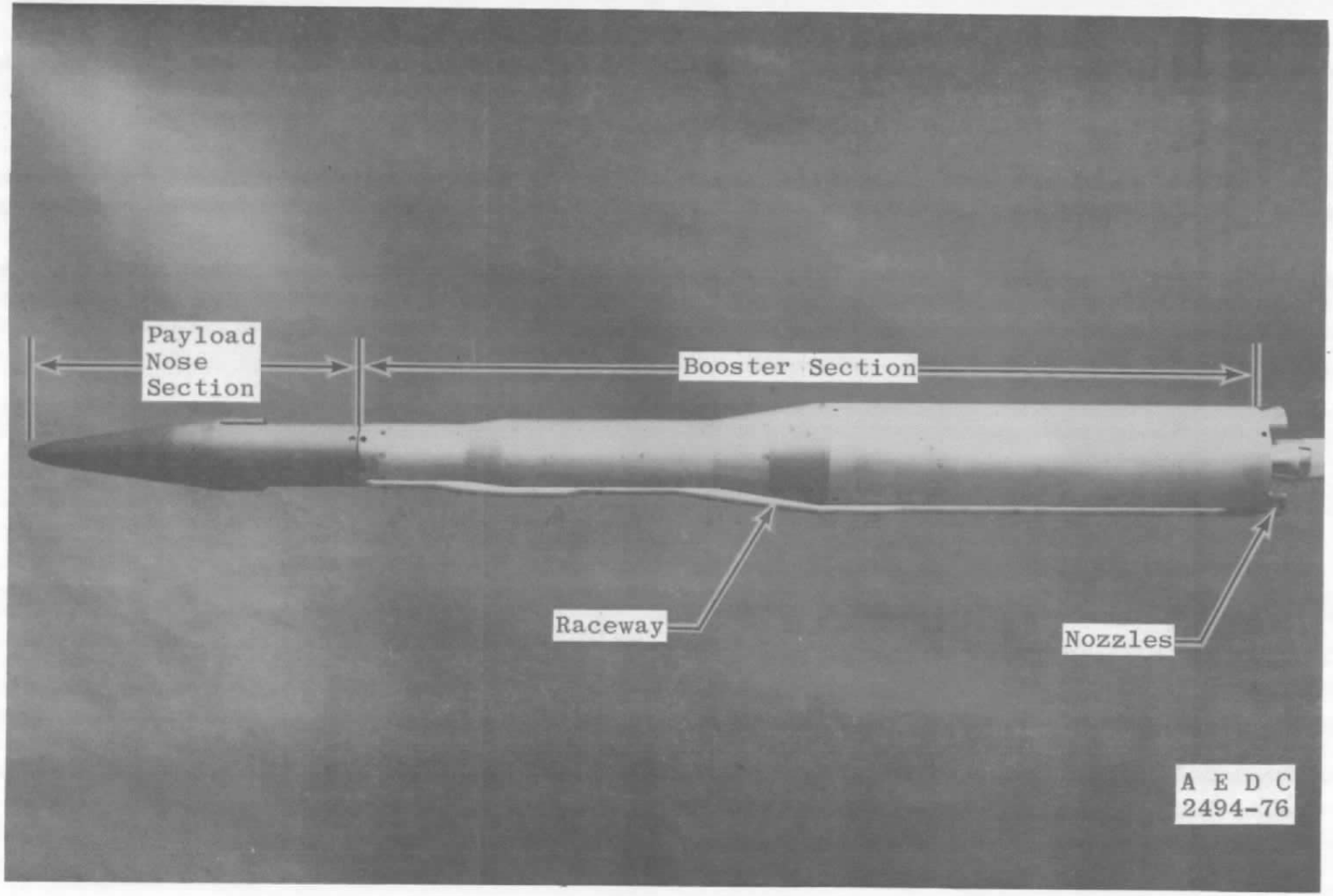

a. Total vehicle

Figure 2. Model photographs.

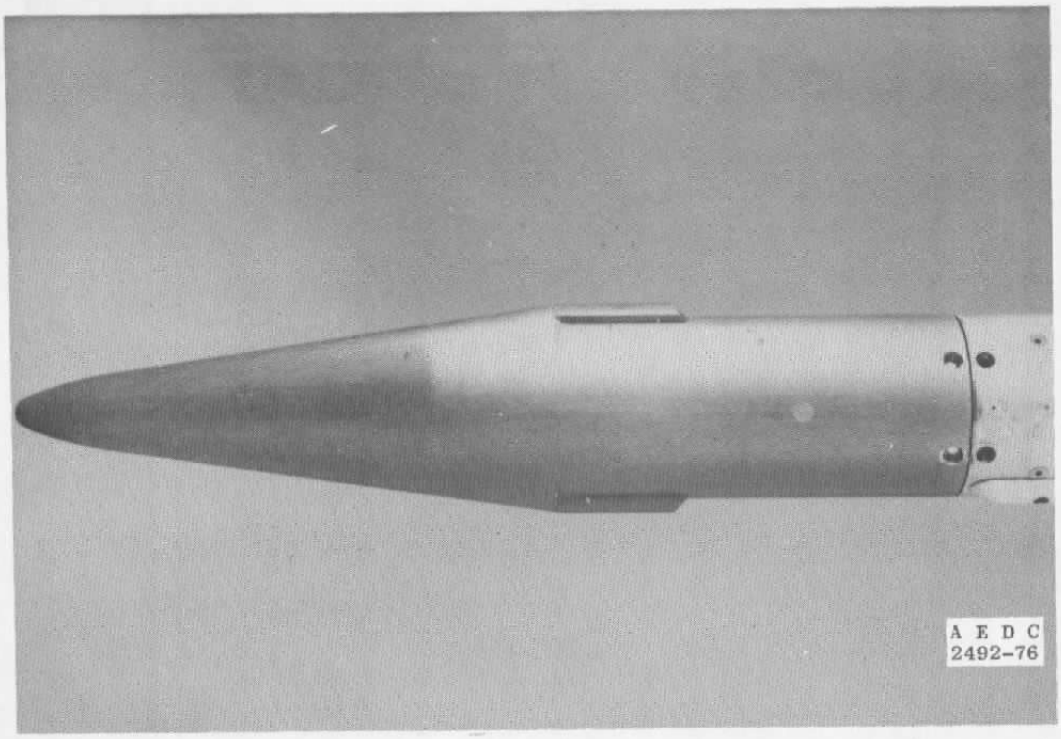

b. Payload nose section

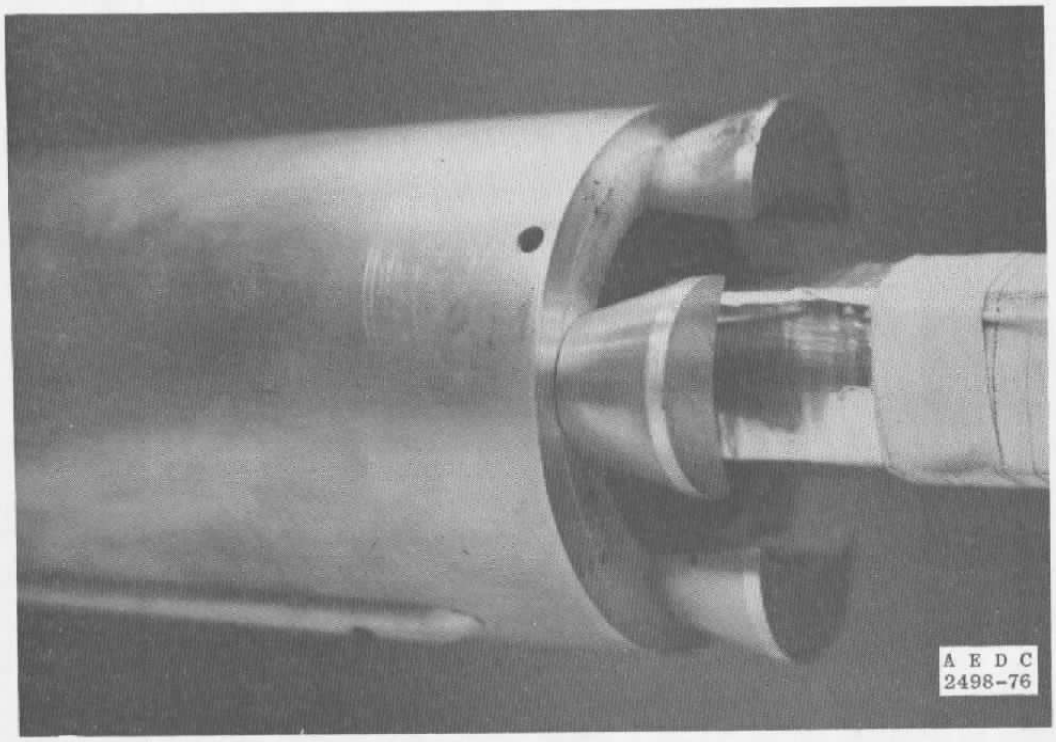

c. Nozzle arrangement
Figure 2. Concluded.

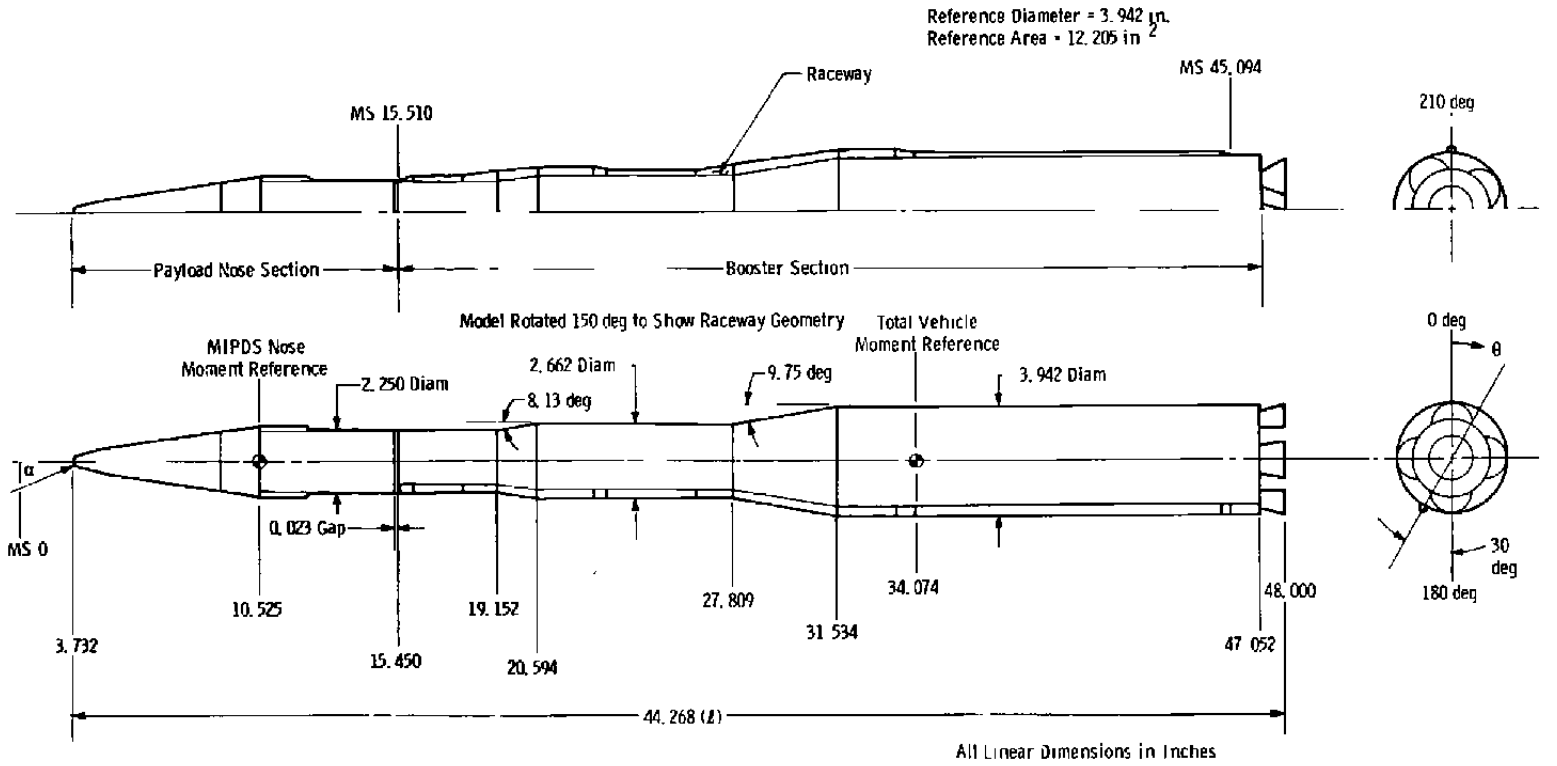

a. Basic model geometry

Figure 3. Model details.

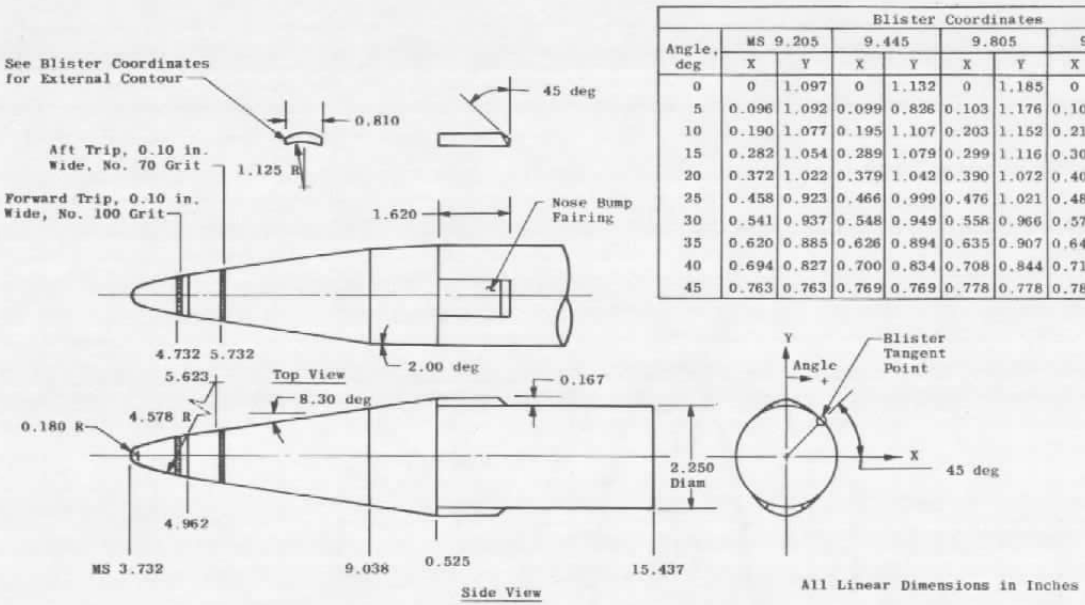

Blister Coordinates										
Angle, deg	MS 9.205		9.445		9.805		9.865		10.525	
	X	Y	X	Y	X	Y	X	Y	X	Y
0	0	1.097	0	1.132	0	1.185	0	1.237	0	1.290
5	0.096	1.092	0.099	0.826	0.103	1.176	0.107	1.227	0.111	1.277
10	0.190	1.077	0.195	1.107	0.203	1.152	0.211	1.197	0.219	1.242
15	0.282	1.054	0.289	1.079	0.299	1.116	0.309	1.154	0.319	1.192
20	0.372	1.022	0.379	1.042	0.390	1.072	0.401	1.102	0.412	1.132
25	0.458	0.923	0.466	0.999	0.476	1.021	0.487	1.045	0.498	1.068
30	0.541	0.937	0.548	0.949	0.558	0.966	0.578	0.984	0.578	1.001
35	0.620	0.885	0.626	0.894	0.635	0.907	0.644	0.920	0.653	0.933
40	0.694	0.827	0.700	0.834	0.708	0.844	0.717	0.854	0.725	0.865
45	0.763	0.763	0.769	0.769	0.778	0.778	0.787	0.787	0.795	0.795

b. Payload nose section

Figure 3. Concluded.

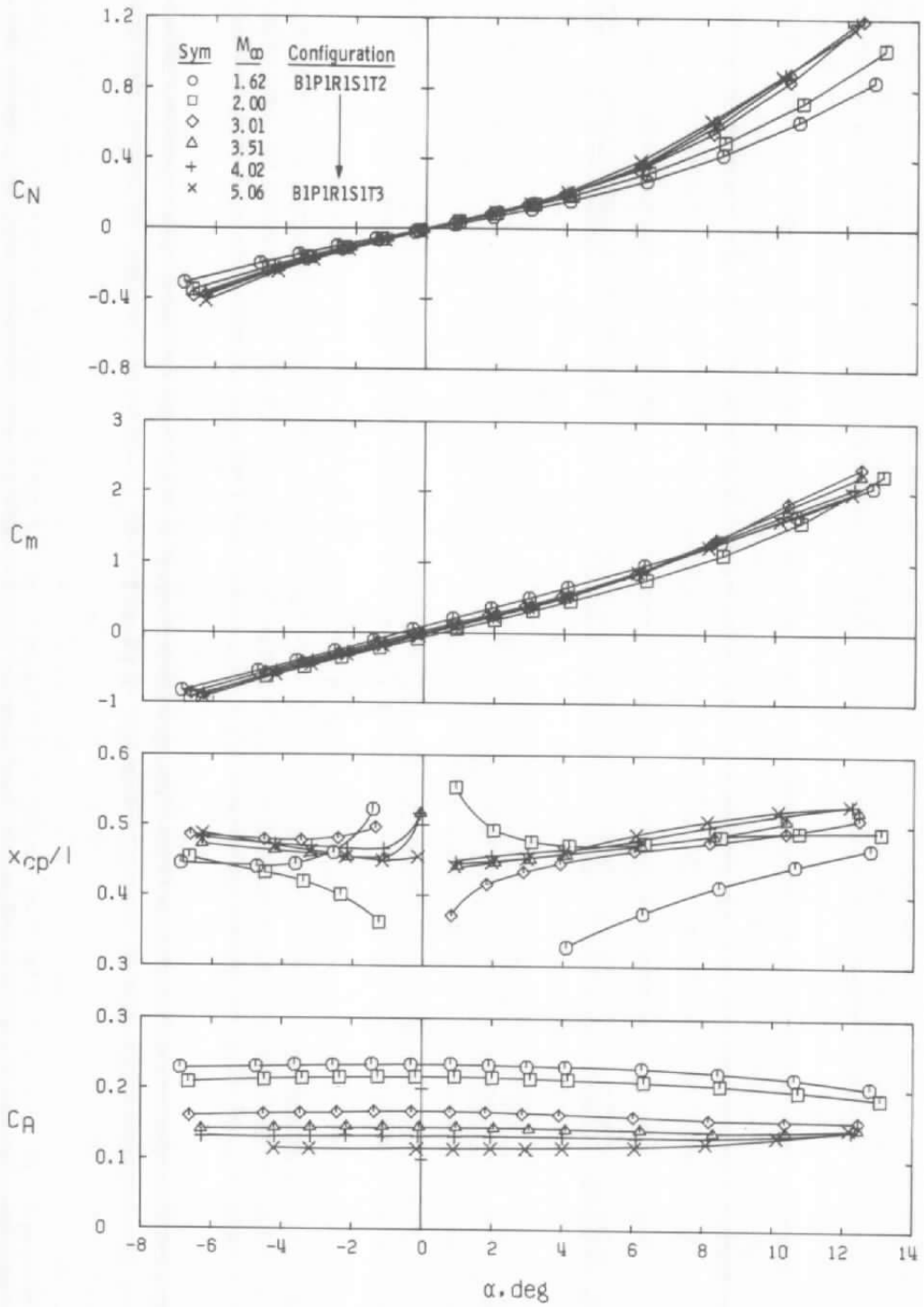

a. Total vehicle

Figure 4. Influence of Mach number on longitudinal stability and axial-force characteristics, ϕ = 0.

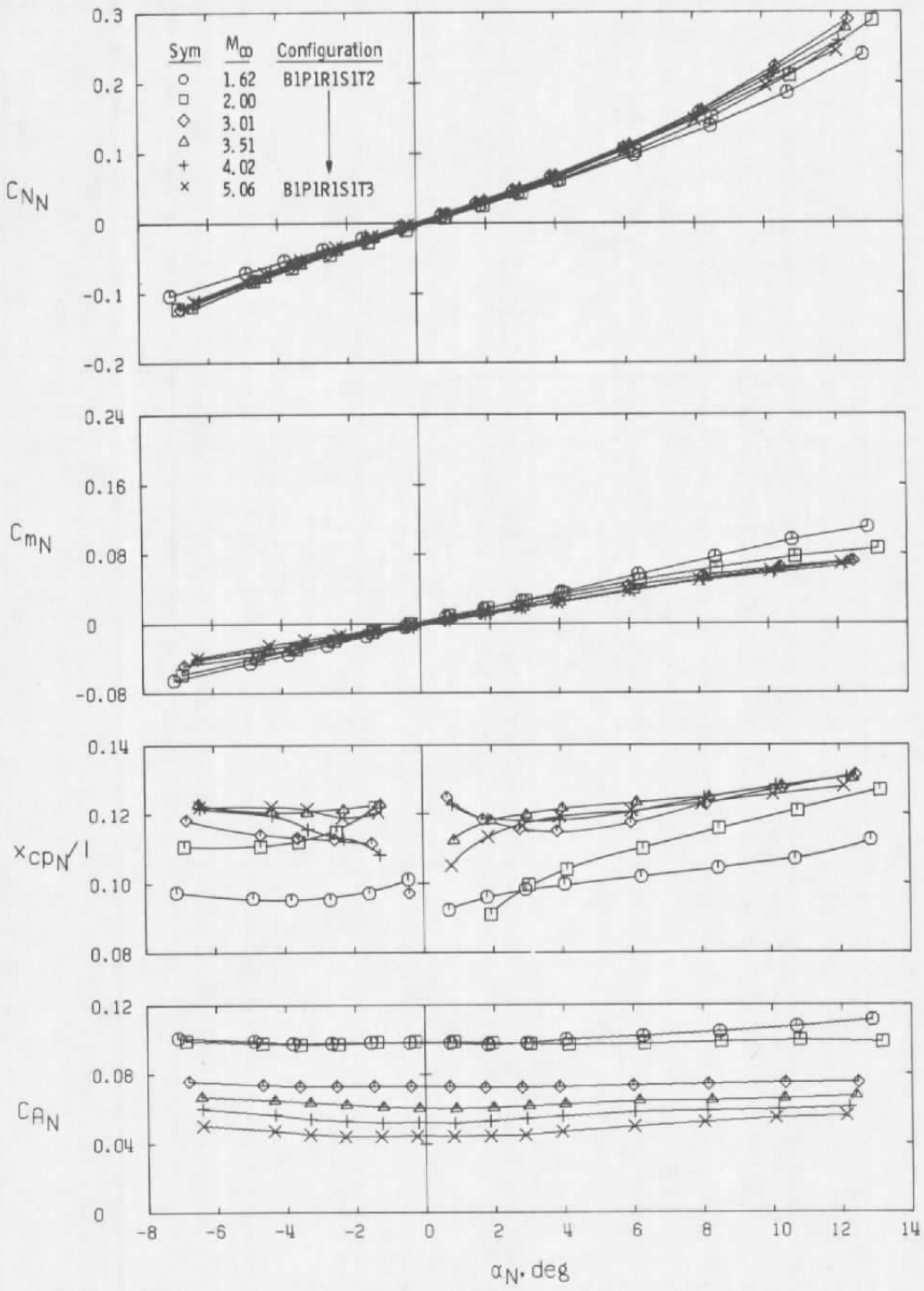

b. Payload nose section

Figure 4. Concluded.

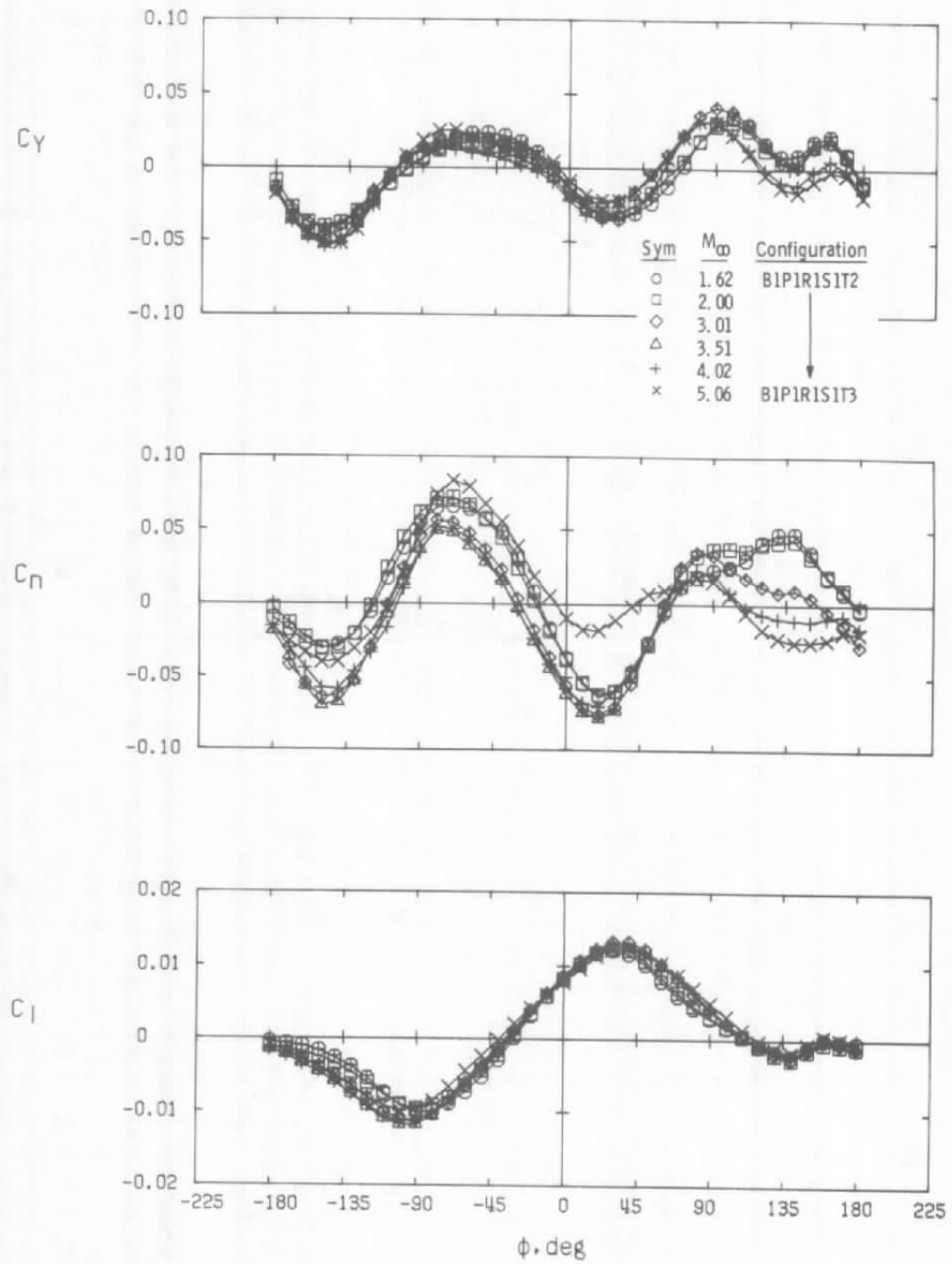

a. Total vehicle

Figure 5. Influence of Mach number on side-force, yawing-moment, and rolling-moment coefficients, α = 6 deg.

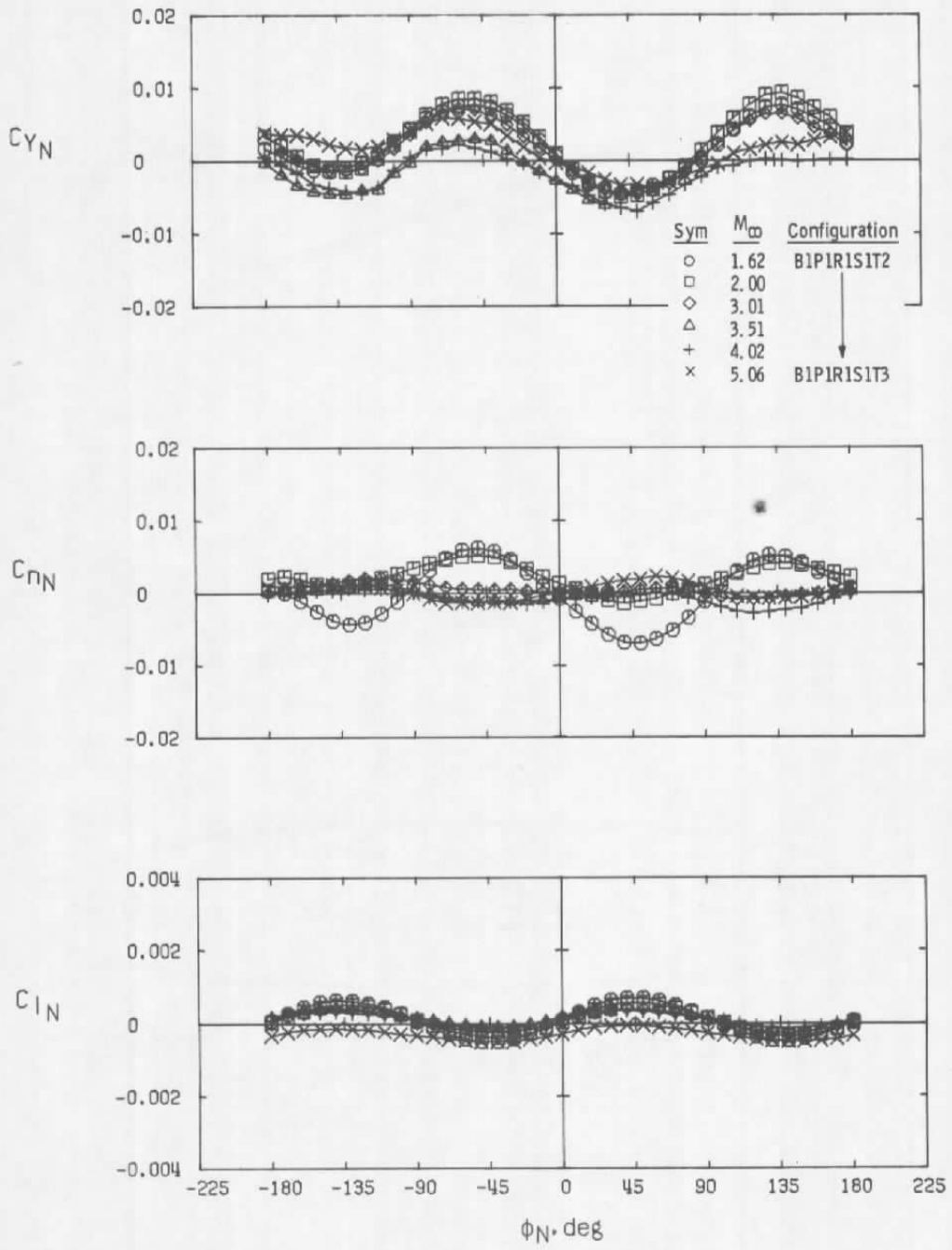

b. Payload nose section

Figure 5. Concluded.

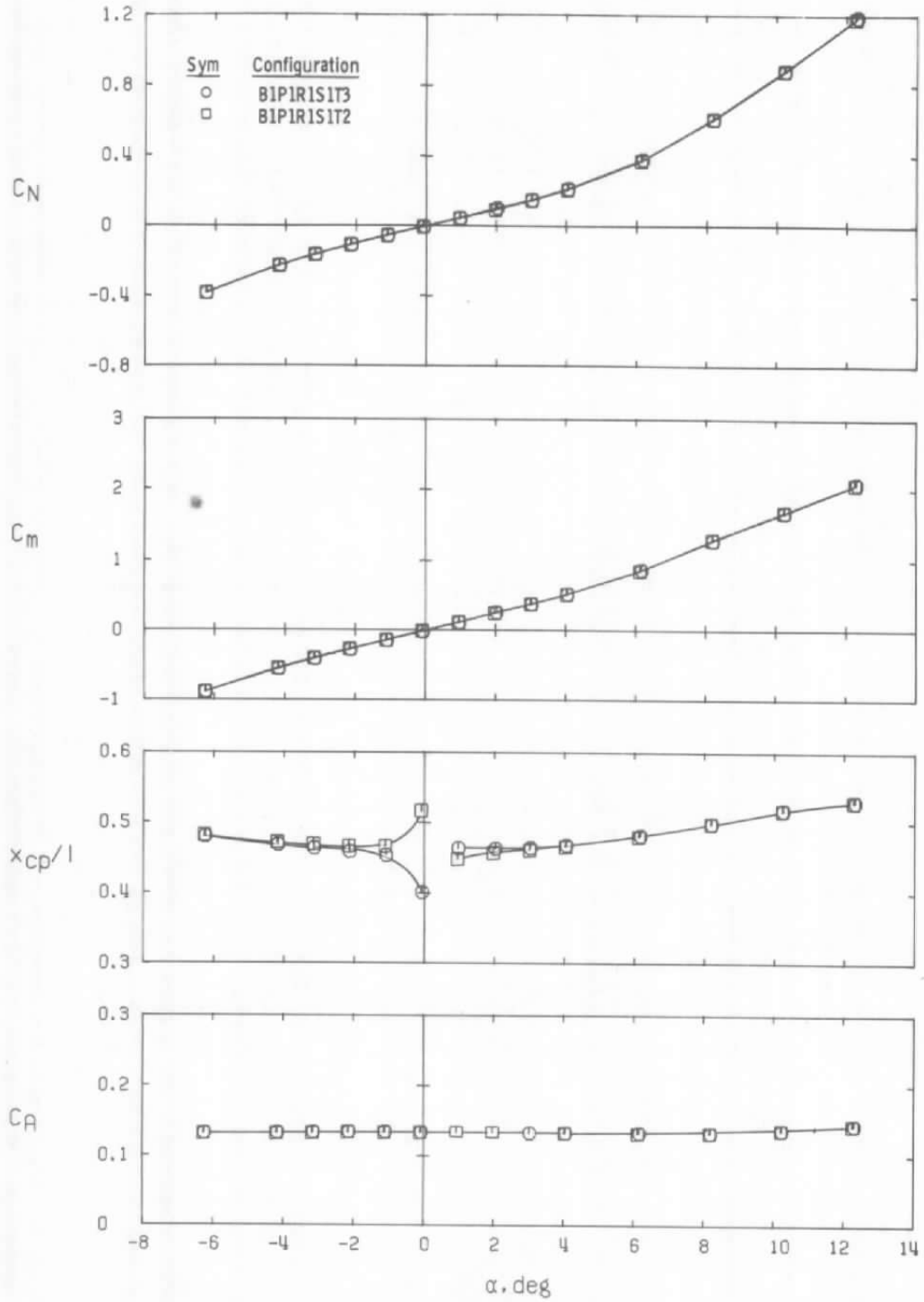

a. Total vehicle

Figure 6. Effect of boundary-layer trip geometry on longitudinal stability and axial-force characteristics, $M_\infty = 4.02$, $\phi = 0$.

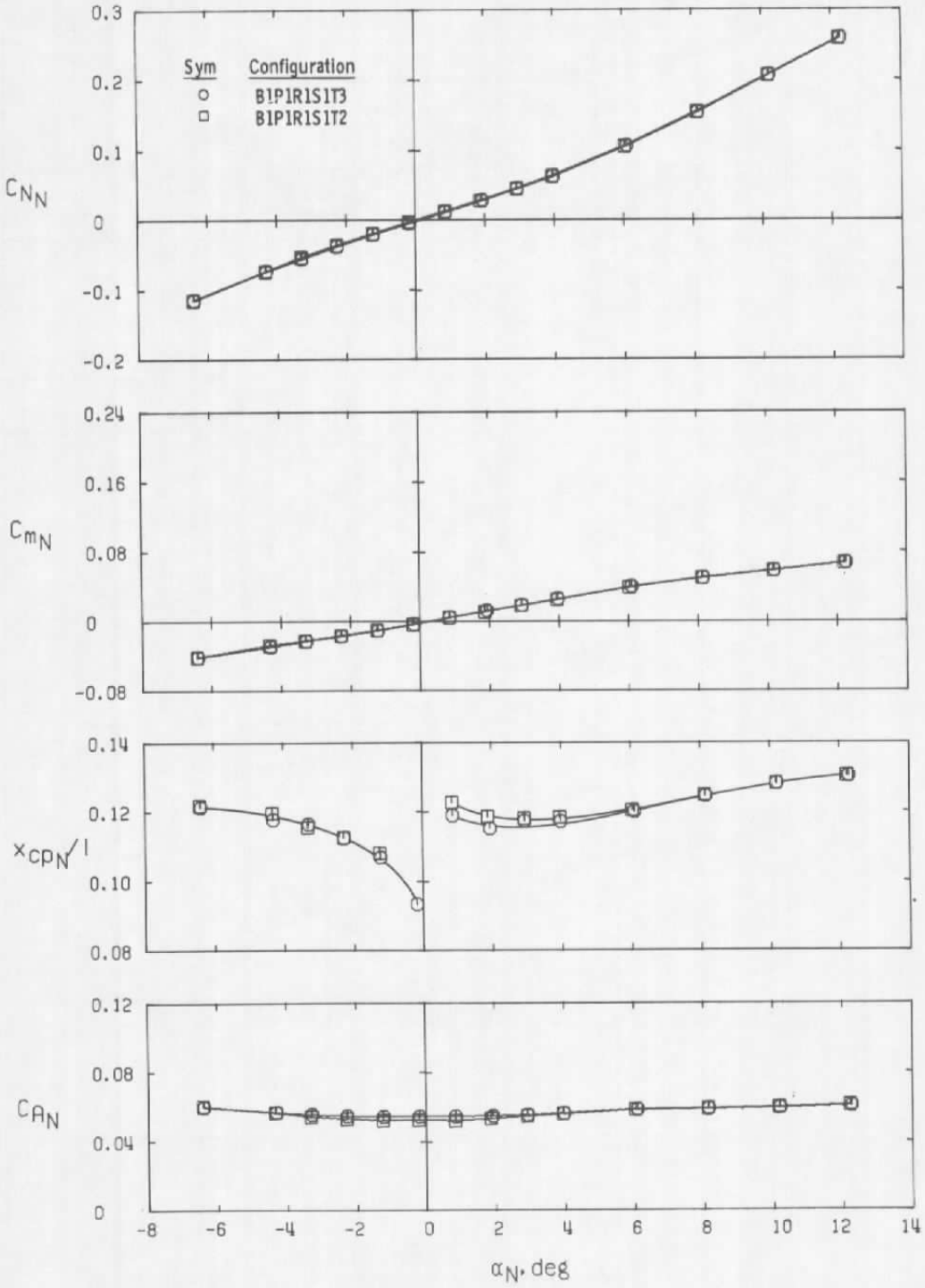

b. Payload nose section

Figure 6. Concluded.

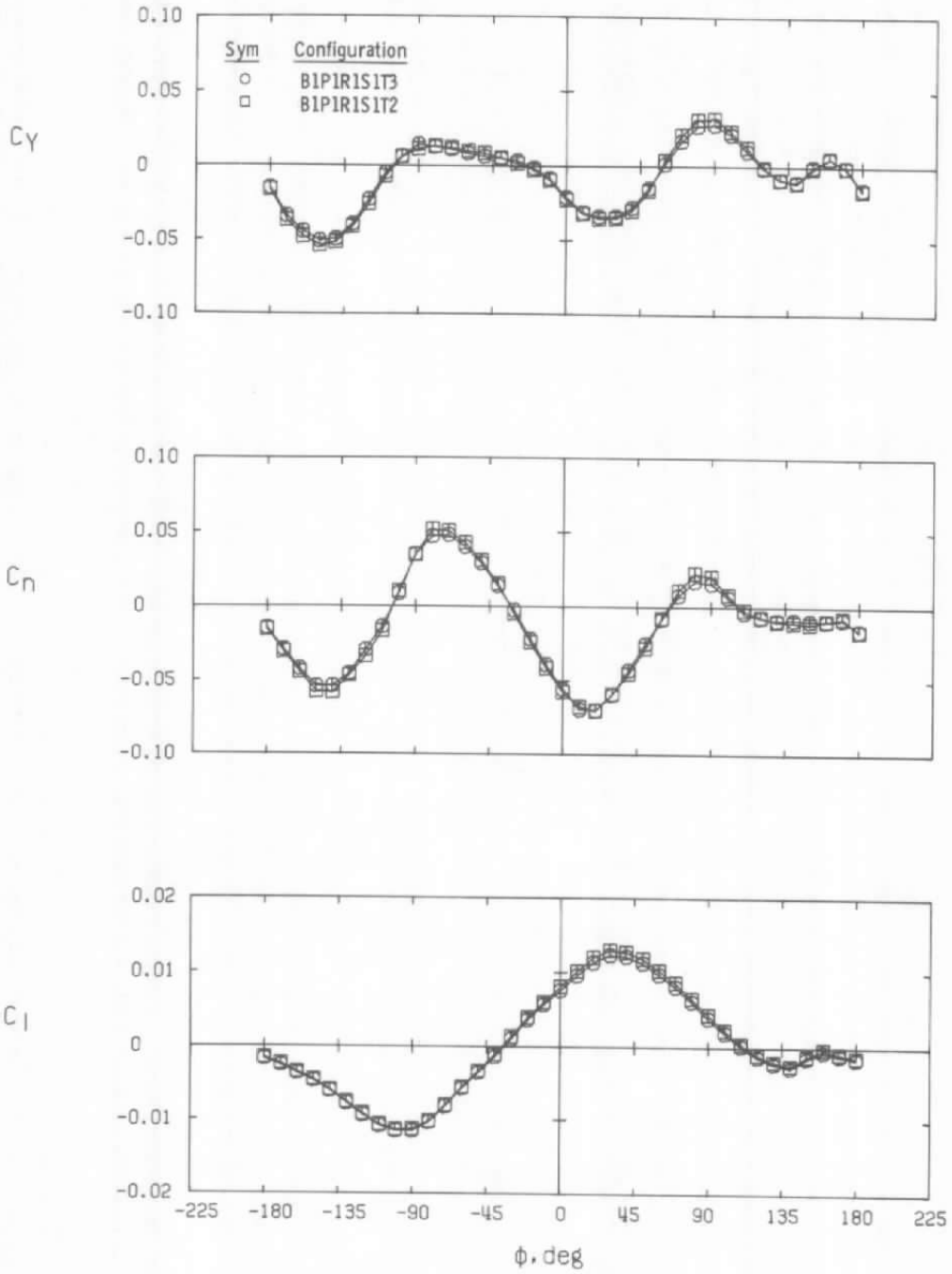

a. Total vehicle

Figure 7. Effect of boundary-layer trip geometry on side-force, yawing-moment, and rolling-moment coefficients, M_∞ = 4.02, α = 6 deg.

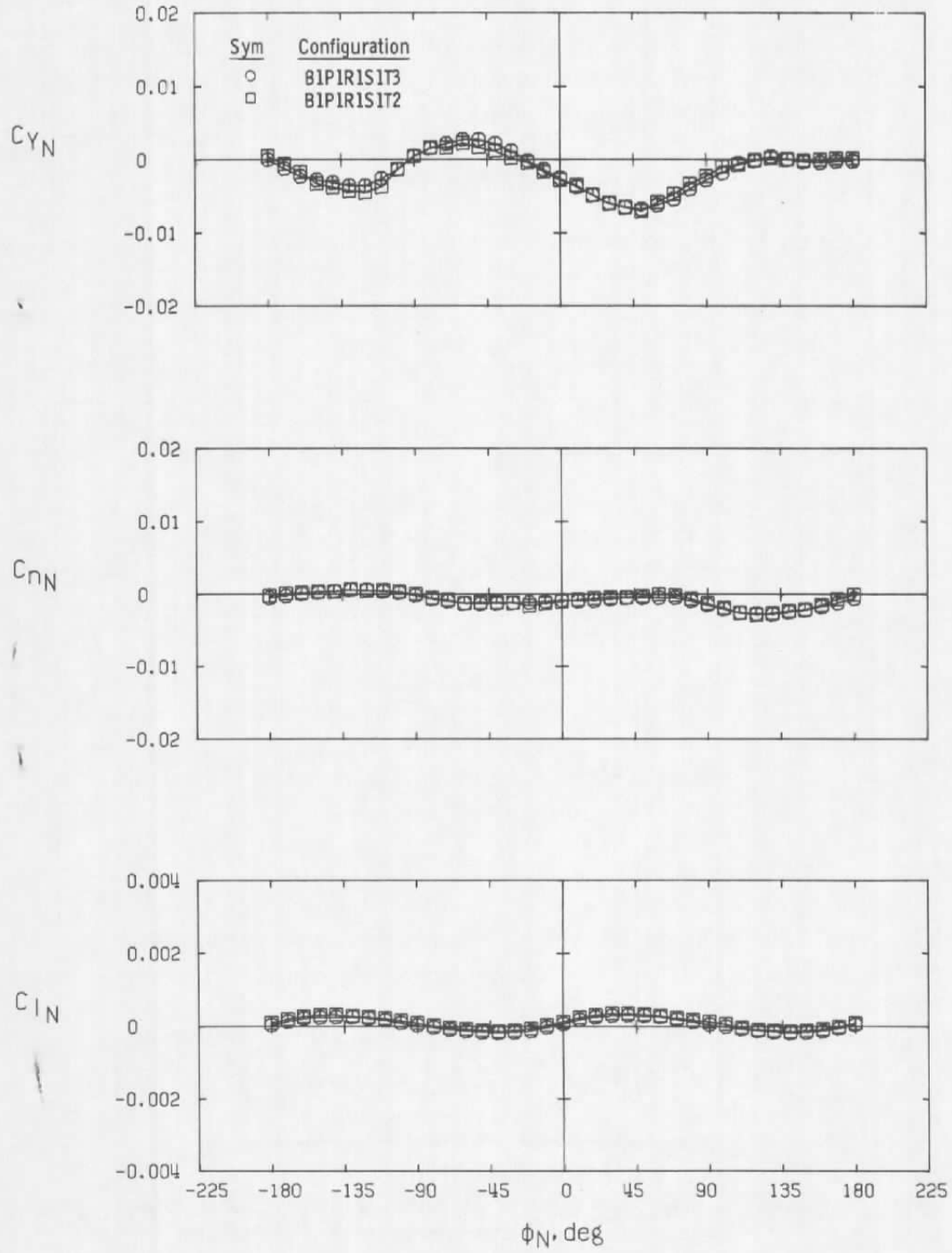

b. Payload nose section

Figure 7. Concluded.

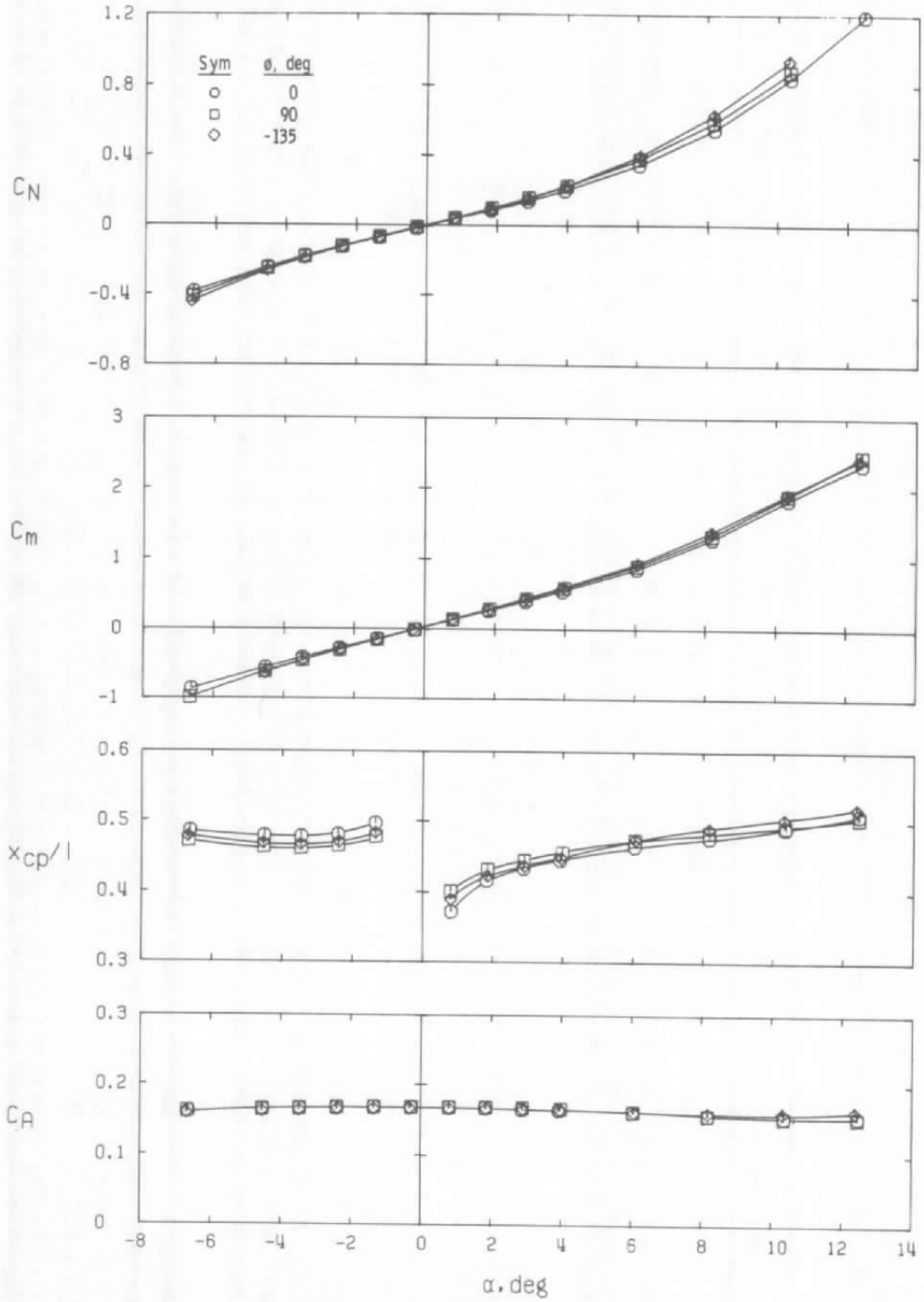

a. Total vehicle

Figure 8. Variations in longitudinal stability and axial-force characteristics with model roll angle, B1P1R1S1T2, M_∞ = 3.01.

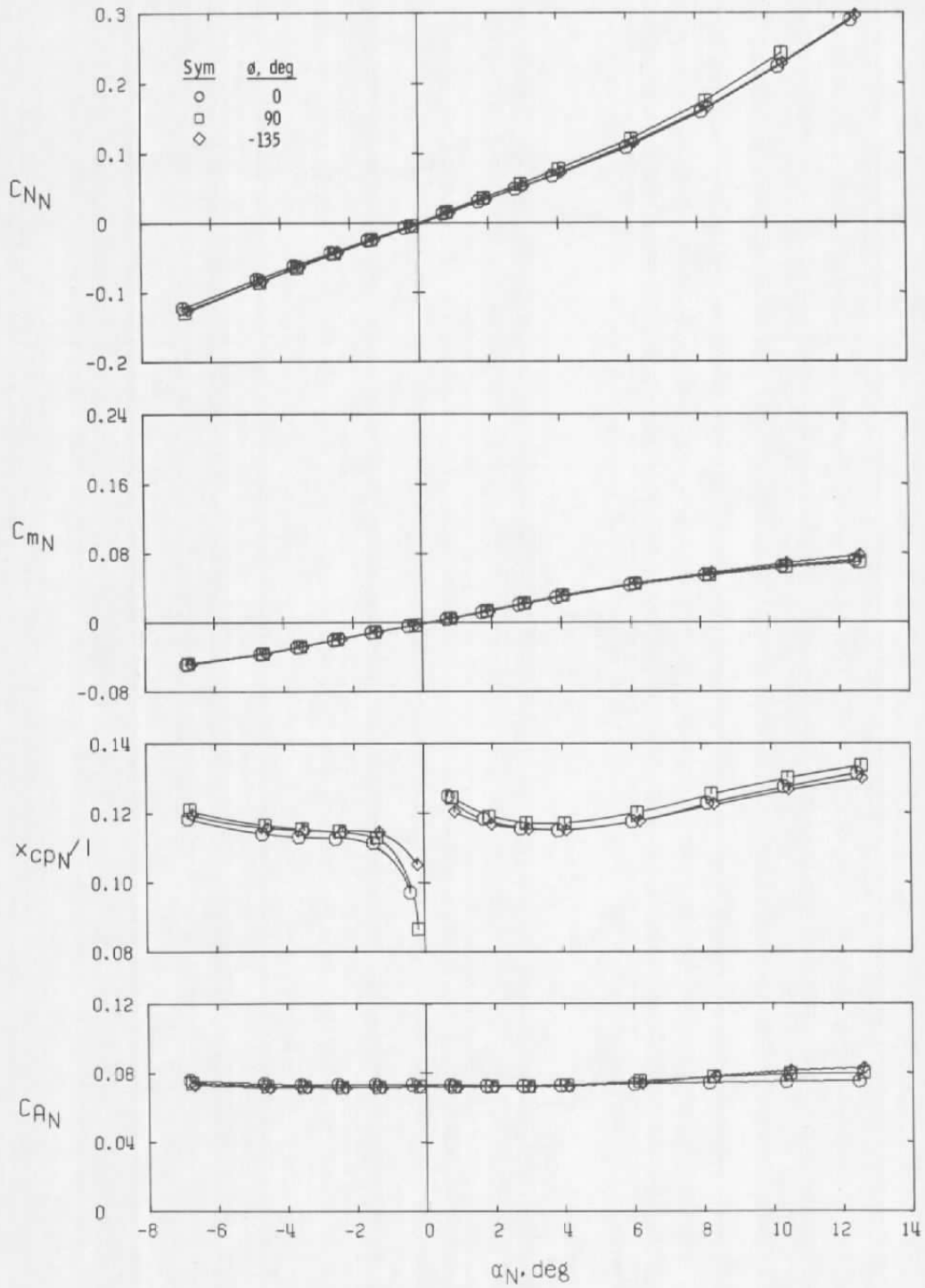

b. Payload nose section
Figure 8. Concluded.

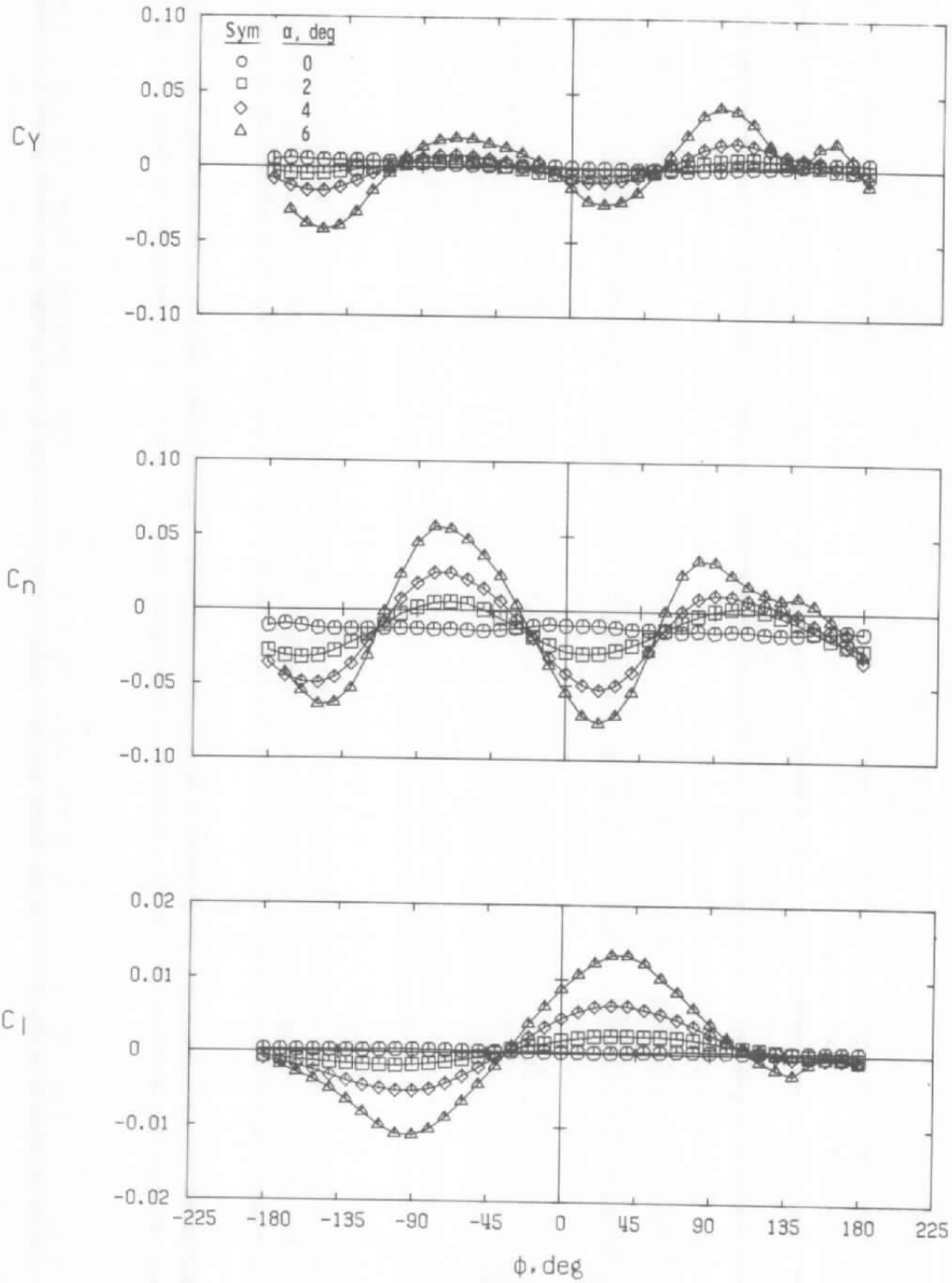

a. Total vehicle

Figure 9. Variations in side-force, yawing-moment and rolling-moment coefficients with model angle of attack, B1P1R1S1T2, M_∞ = 3.01.

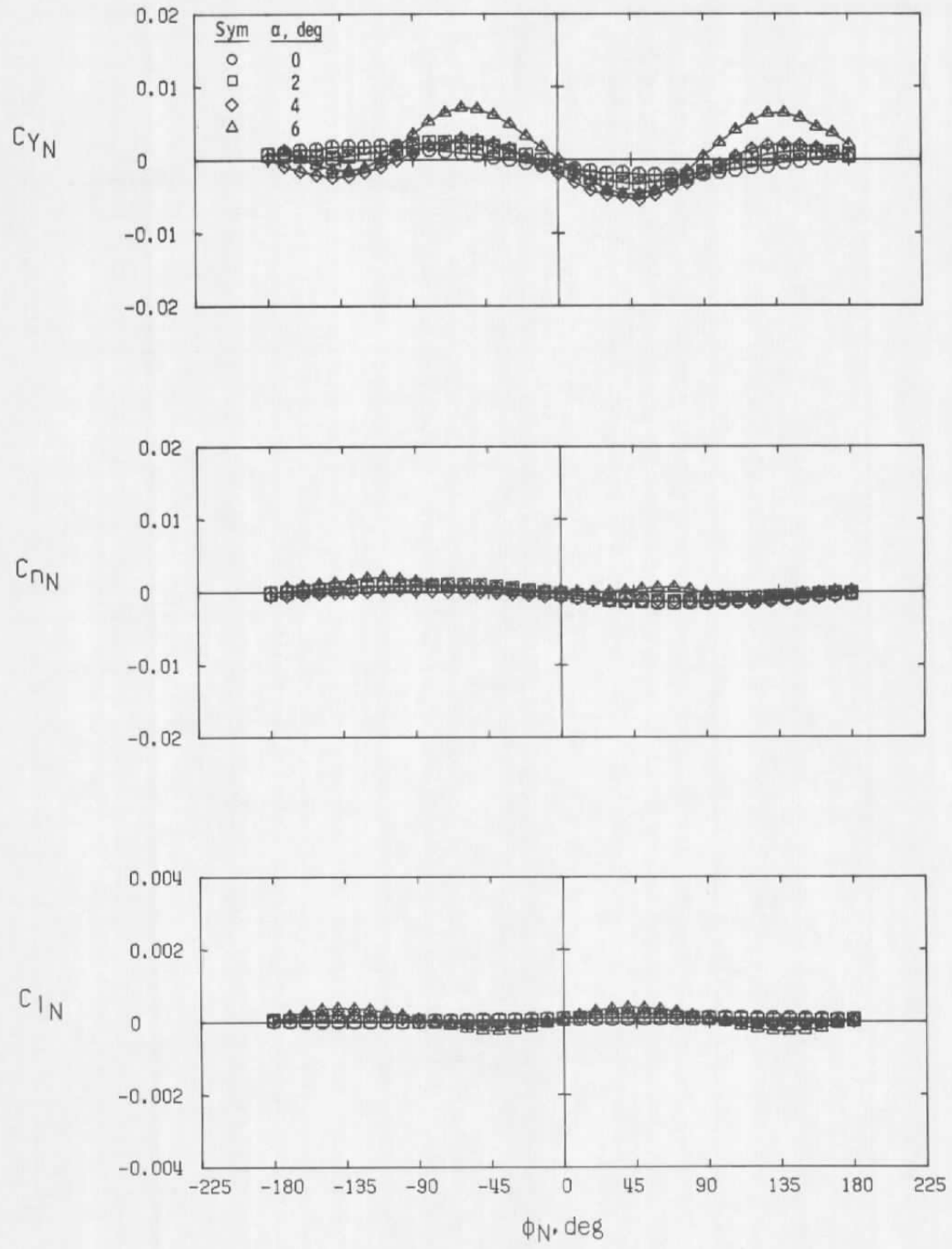

b. Payload nose section
Figure 9. Concluded.

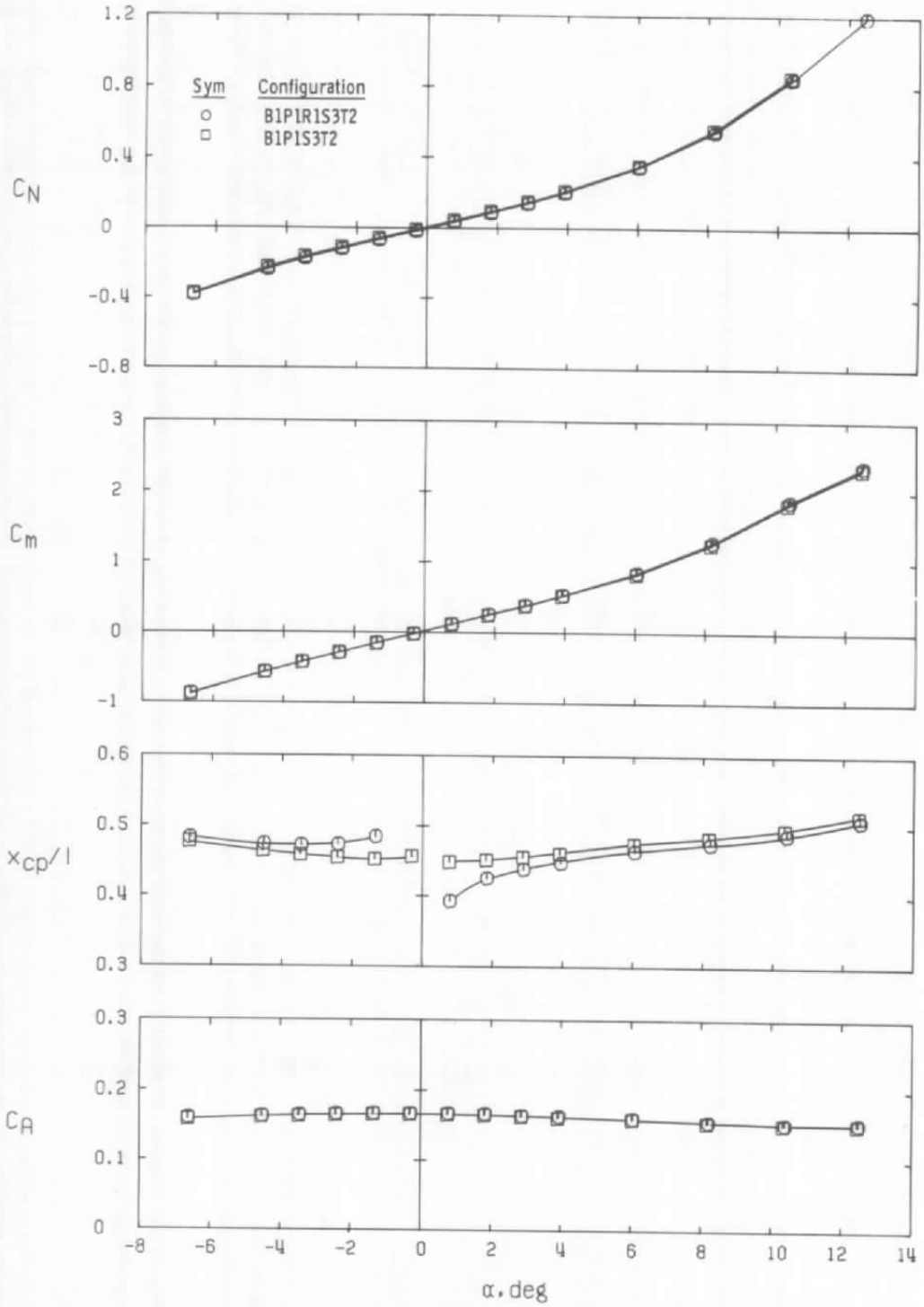

a. Longitudinal stability and axial-force characteristics

Figure 10. Effect of booster raceway on total vehicle aerodynamic characteristics, $M_\infty = 3.01$.

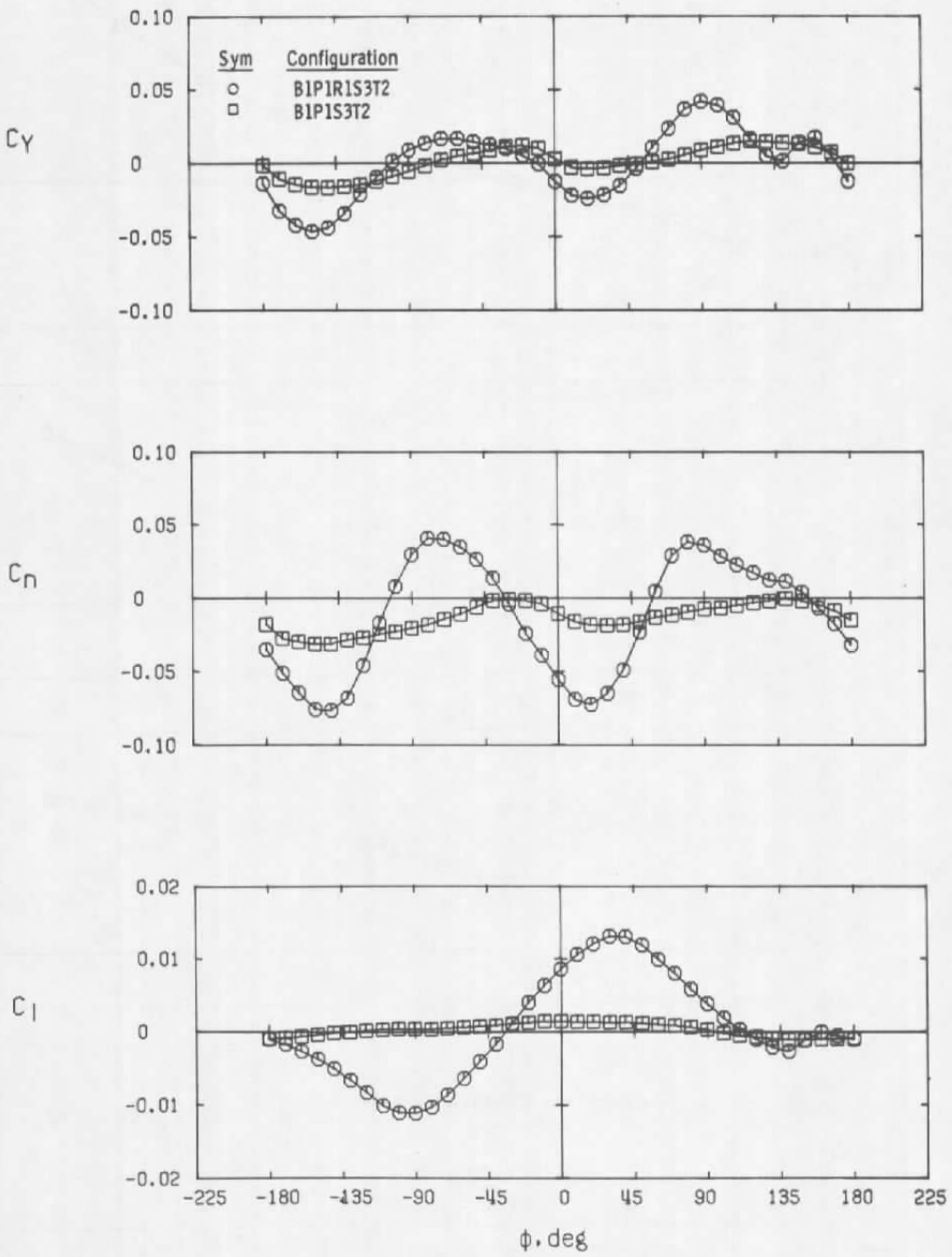

b. Side-force, yawing-moment, and rolling-moment coefficients, α = 6 deg
Figure 10. Concluded.

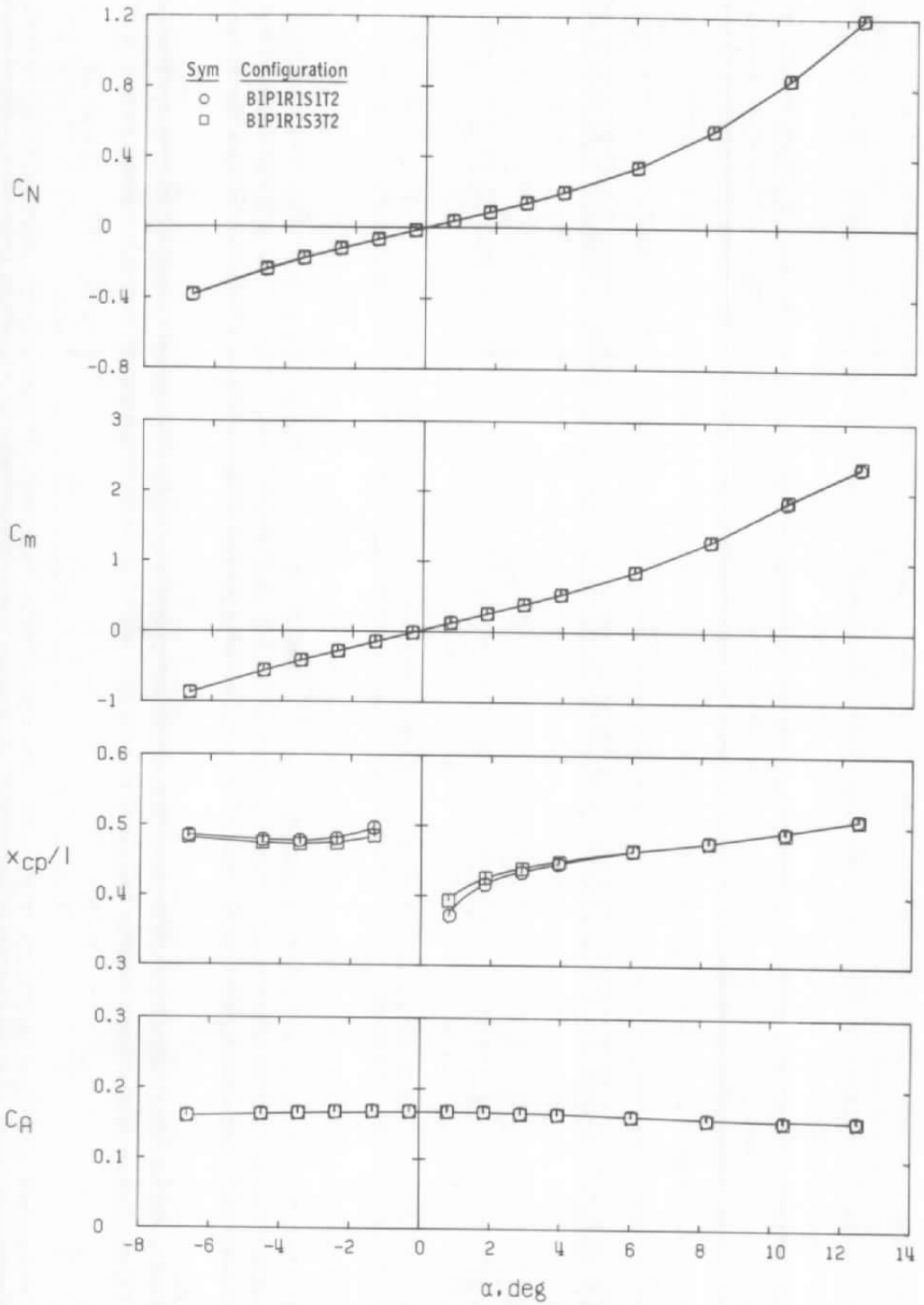

a. Longitudinal stability and axial-force characteristics

Figure 11. Effect of open seal on total vehicle aerodynamic characteristics, $M_\infty = 3.01$.

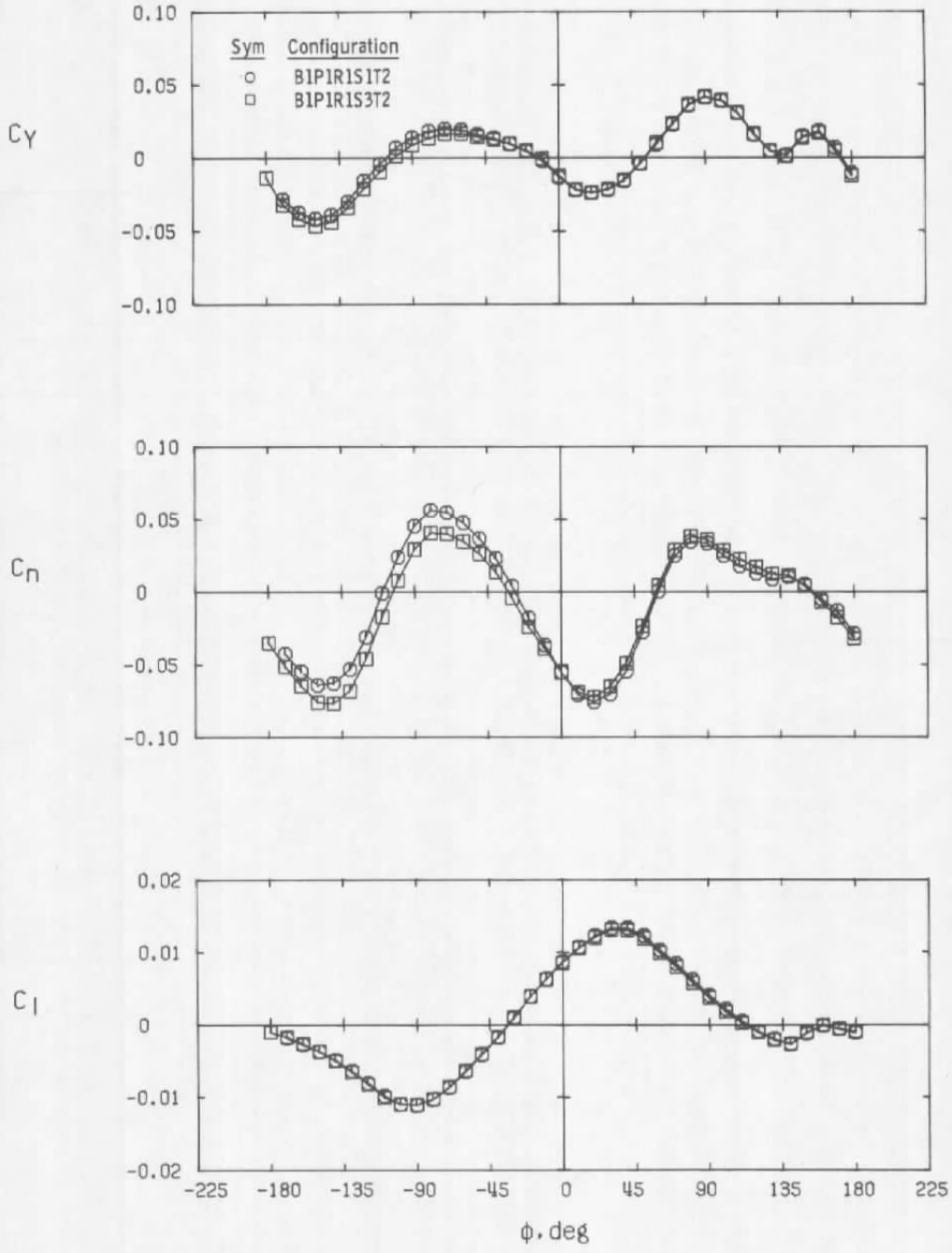

b. Side-force, yawing-moment, and rolling-moment coefficients, α = 6 deg
Figure 11. Concluded.

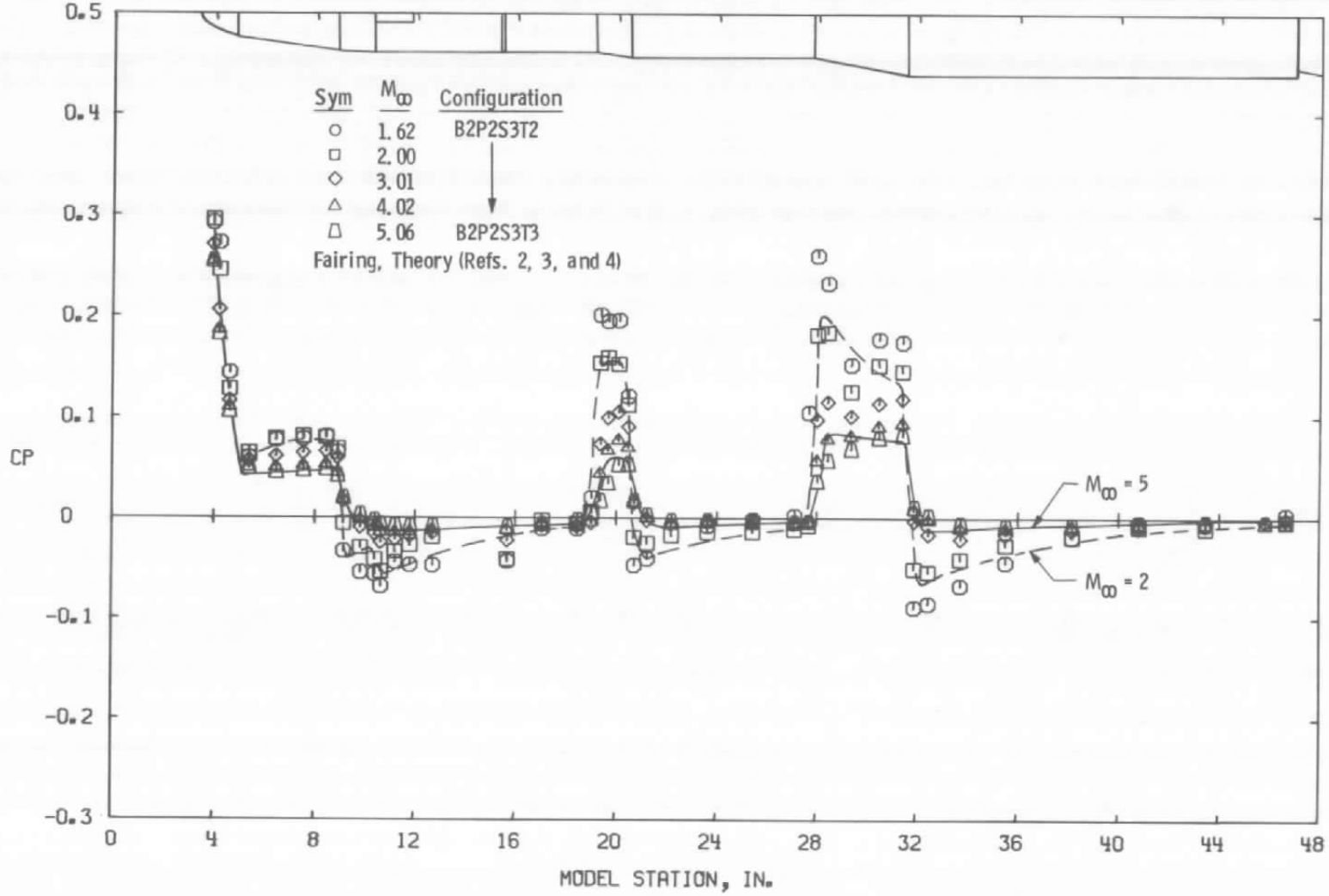

Figure 12. Variation in longitudinal surface pressure distribution with Mach number, θ = 90 deg, α = 0.

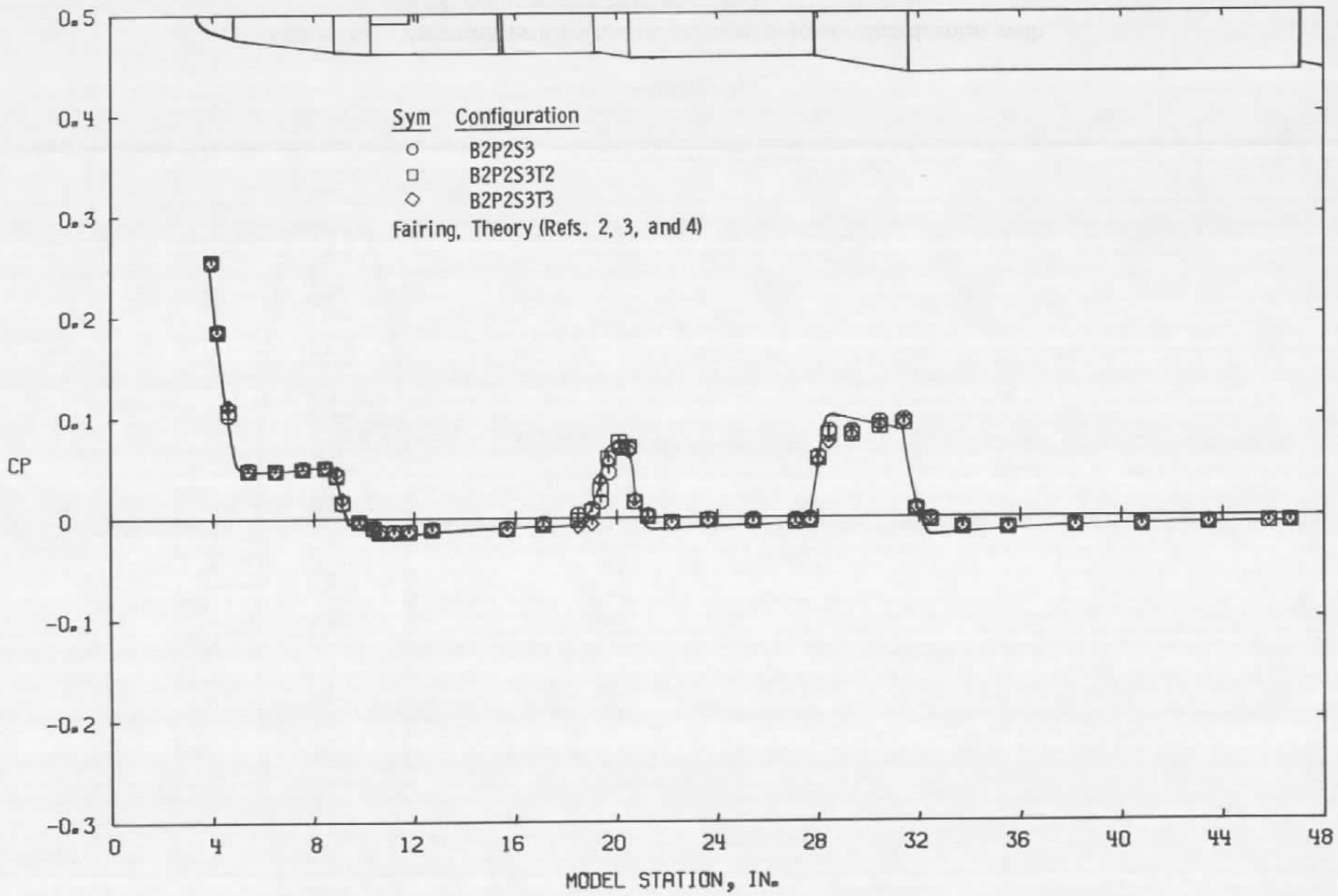

Figure 13. Effect of boundary-layer trip geometry on longitudinal surface pressure distribution, M_∞ = 4.02, θ = 90 deg, α = 0.

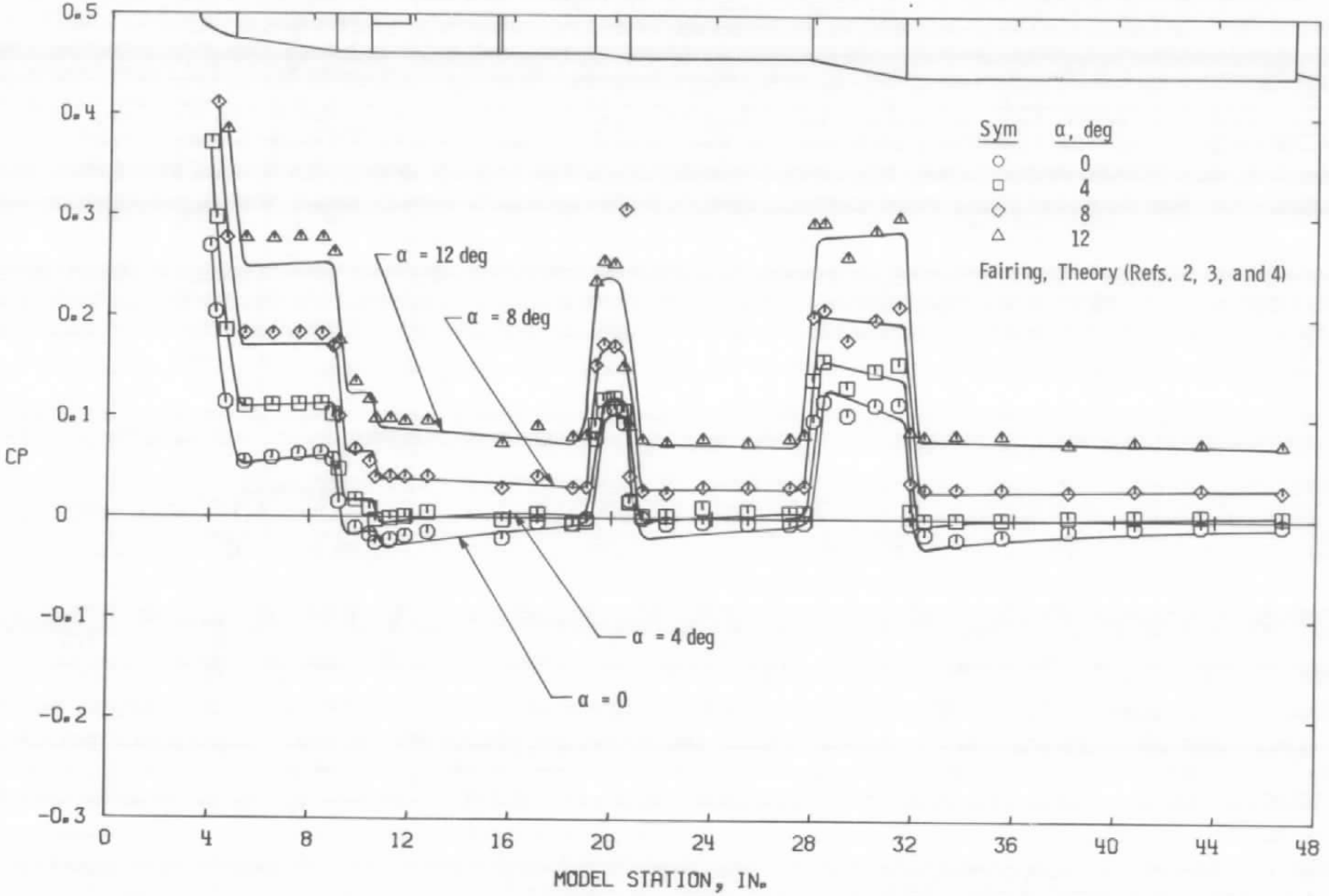

Figure 14. Angle-of-attack influence on longitudinal surface pressure distribution, B2P2S3T2, M_∞ = 3.01, θ = 90 deg, ϕ = 90 deg.

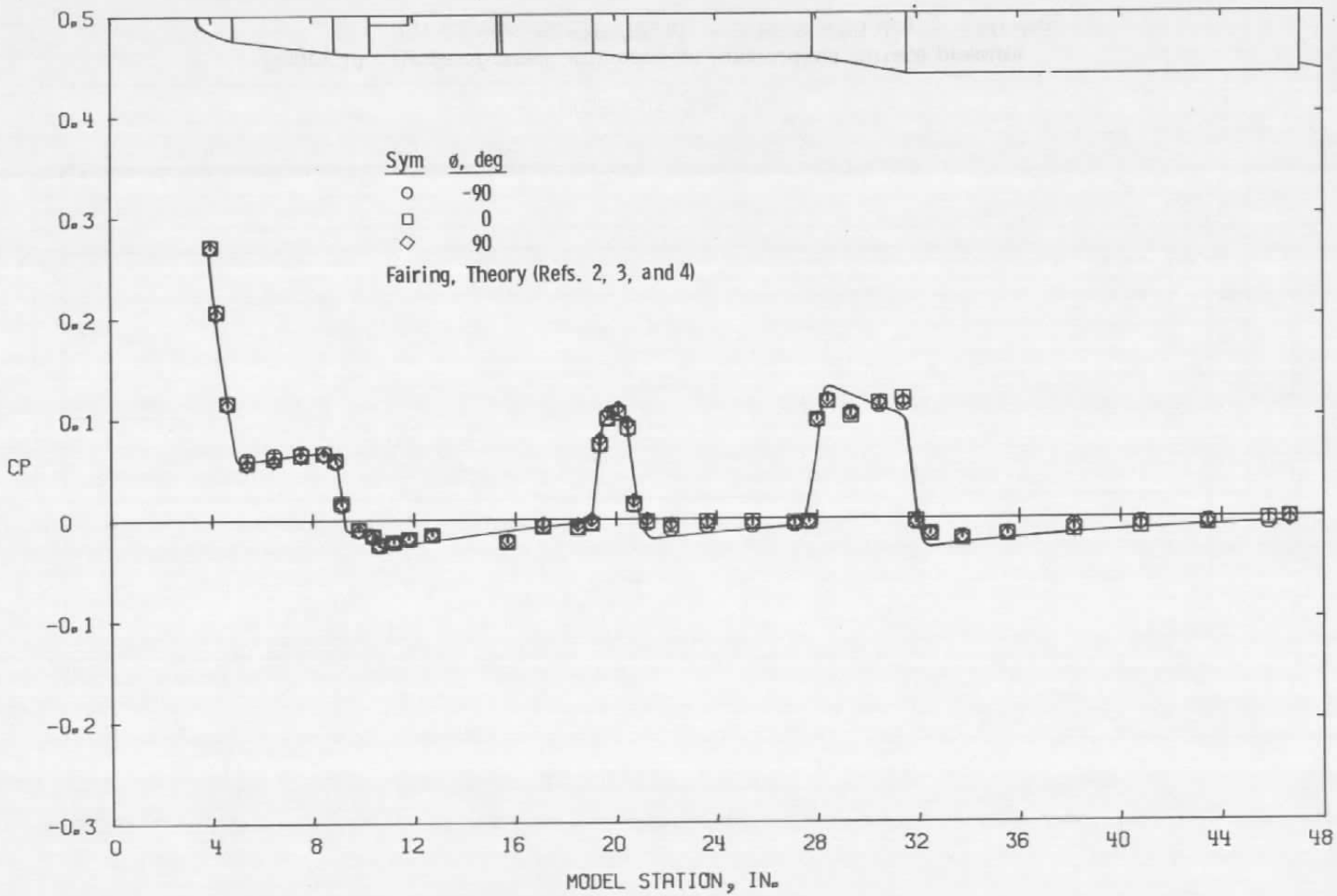

Figure 15. Repeatability of longitudinal surface pressure distribution data, B2P2S3T2, M_∞ = 3.01, θ = 90 deg, α = 0.

Table 1. Pressure Orifice Locations

Model Station	X/ℓ	Orifice Circumferential Location, θ, deg								
		90	105	120	135	150	159	165	180	270
3.960	0.005	x								
4.200	0.011	x								
4.620	0.020	x								
5.400	0.038	x								
6.480	0.062	x								
7.560	0.086	x								x
8.460	0.107	x								
8.918	0.117	x								
9.158	0.123	x								
9.840	0.138	x	x	x	x	x		x	x	x
10.405	0.151	x							x	
10.525	0.153						x			
10.645	0.156	x							x	
11.220	0.169	x	x	x	x	x	x	x	x	x
11.820	0.183	x							x	
12.063	0.188								x	
12.720	0.203	x	x	x	x	x		x	x	x
14.160	0.236	x	x	x	x	x		x	x	x
15.685	0.270	x								x
17.100	0.302	x								
18.480	0.333	x								
19.032	0.346	x								
19.370	0.351	x								
19.680	0.360	x								
20.100	0.370	x		x		x			x	x
20.474	0.378	x								
20.714	0.384	x								
21.240	0.396	x								
22.200	0.417	x								x
23.640	0.450	x								
25.440	0.490	x								
27.120	0.528	x								
27.684	0.541	x								
28.020	0.549	x								
28.440	0.558	x								
29.370	0.579	x								
30.480	0.604	x		x		x			x	x
31.414	0.625	x								
31.904	0.636	x								
32.470	0.649	x								
33.730	0.678	x								
35.530	0.718	x								x
38.170	0.778	x								
40.810	0.838	x								
43.450	0.897	x								
45.840	0.951	x								
46.680	0.970	x								
47.052	0.979	Base Pressures - (θ = 45, 135, 225, and 315 deg)								

Table 2. Force Test Summary

CONFIGURATION	α, deg	ϕ, deg	Mach Number 1.62	2.00	3.01	3.51	3.76	4.02	5.06
B1P1R1S1T3	D	0						x	x
		90						x	x
		-135						x	x
		-180							x
	-4	R						x	x
	0							x	x
	2							x	x
	4							x	x
	6							x	x
	8							x	x
	12							x	x
B1P1R1S1T2	D	0	x	x	x	x		x	
		90	x	x	x	x		x	
		-135	x	x	x	x		x	
		-180	x	x	x	x		x	
	-4	R				x		x	
	0		x	x	x	x		x	
	2		x	x	x	x		x	
	4		x	x	x	x		x	
	6		x	x	x	x		x	
	8							x	
	12							x	
B1P1R1S3T2 (*)	D	0	x	x	x		x	x	
		90	x	x	x		x	x	
		-135	x	x	x			x	
	0	R	x	x	x			x	
	4		x	x				x	
	6		x	x	x			x	
B1P1S3T2 (*)	D	0	x	x	x			x	
		90	x	x	x			x	
		-135	x	x	x			x	
	0	R	x	x	x			x	
	4		x	x	x			x	
	6		x		x				

Notes:
1. Angle-of-attack schedule D: α = -6,-4,-3,-2,-1,0, 1,2,3,4,6,8,10,12 deg (Pitch-pause mode)
2. Roll angle schedule R: ϕ = -180 to 180 deg (Continuous sweep mode)
3. Asterisk (*) indicates data obtained only for total vehicle configuration

Table 3. Pressure Test Summary

CONFIGURATION	Mach No.	α, deg	Roll Angle, ϕ, deg													
			-90	-75	-60	-45	-30	-15	0	15	30	45	60	75	90	180
B2P2S3T3	5.06	-4	x						x	x	x	x	x	x	x	x
		-2	x						x	x	x	x	x	x	x	x
		0	x						x	x	x	x	x	x	x	x
		2	x						x	x	x	x	x	x	x	x
		4	x						x	x	x	x	x	x	x	x
B2P2S3T3	4.02	-4	x						x	x	x	x	x	x	x	x
		-2	x						x	x	x	x	x	x	x	x
		0	x						x	x	x	x	x	x	x	x
		2	x						x	x	x	x	x	x	x	x
		4	x						x	x	x	x	x	x	x	x
B2P2S3T2	4.02	-4	x	x	x	x	x	x	x	x	x	x	x	x	x	x
		-2	x	x	x	x	x	x	x	x	x	x	x	x	x	x
		0	x	x	x	x	x	x	x	x	x	x	x	x	x	x
		2	x	x	x	x	x	x	x	x	x	x	x	x	x	x
		4	x	x	x	x	x	x	x	x	x	x	x	x	x	x
B2P2S3	4.02	-4	x						x						x	x
		0	x						x						x	x
		12	x						x						x	x
B2P2S3T2	3.01	-12	x	x	x	x	x	x	x	x	x	x	x	x	x	x
		-8	x	x	x	x	x	x	x	x	x	x	x	x	x	x
		-4	x	x	x	x	x	x	x	x	x	x	x	x	x	x
		-2	x	x	x	x	x	x	x	x	x	x	x	x	x	x
		0	x	x	x	x	x	x	x	x	x	x	x	x	x	x
		2	x	x	x	x	x	x	x	x	x	x	x	x	x	x
		4	x	x	x	x	x	x	x	x	x	x	x	x	x	x
		8	x	x	x	x	x	x	x	x	x	x	x	x	x	x
		12	x	x	x	x	x	x	x	x	x	x	x	x	x	x
B2P2S3T2	2.00	-12	x						x	x	x	x	x	x	x	x
		-8	x						x	x	x	x	x	x	x	x
		-4	x						x	x	x	x	x	x	x	x
		-2	x						x	x	x	x	x	x	x	x
		0	x						x	x	x	x	x	x	x	x
		2	x						x	x	x	x	x	x	x	x
		4	x						x	x	x	x	x	x	x	x
		8	x						x	x	x	x	x	x	x	x
		12	x						x	x	x	x	x	x	x	x
B2P2S3T2	1.62	-12	x						x	x	x	x	x	x	x	x
		-8	x						x	x	x	x	x	x	x	x
		-4	x						x	x	x	x	x	x	x	x
		-2	x						x	x	x	x	x	x	x	x
		0	x						x	x	x	x	x	x	x	x
		2	x						x	x	x	x	x	x	x	x
		4	x						x	x	x	x	x	x	x	x
		8	x						x	x	x	x	x	x	x	x
		12	x						x	x	x	x	x	x	x	x
B2P2S3	1.62	-4													x	
		0													x	
		4													x	

NOMENCLATURE

C_A	Total vehicle axial-force coefficient
C_{A_N}	Nose section axial-force coefficient
C_ℓ	Total vehicle rolling-moment coefficient
C_{ℓ_N}	Nose section rolling-moment coefficient
C_m	Total vehicle pitching-moment coefficient
C_{m_N}	Nose section pitching-moment coefficient
C_N	Total vehicle normal-force coefficient
C_{N_N}	Nose section normal-force coefficient
C_n	Total vehicle yawing-moment coefficient
C_{n_N}	Nose section yawing-moment coefficient
CP	Pressure coefficient
C_Y	Total vehicle side-force coefficient
C_{Y_N}	Nose section side-force coefficient
d	Reference diameter, 3.942 in.
ℓ	Model length, 44.268 in.
M_∞	Free-stream Mach number
p_o	Tunnel stilling chamber pressure, psia
p_∞	Free-stream static pressure, psia
q_∞	Free-stream dynamic pressure, psia
Re_∞	Free-stream unit Reynolds number, ft^{-1}
S	Reference area, 12.205 $in.^2$
T_o	Tunnel stilling chamber temperature, °R

X_{cp}/ℓ Total vehicle axial center-of-pressure location from model nose, ratioed to model length

X_{cp_N}/ℓ Nose section axial center-of-pressure location from model nose, ratioed to model length

α Total vehicle angle of attack, deg

α_N Nose section angle of attack, deg

ϕ Total vehicle roll angle, deg

ϕ_N Nose section roll angle, deg

θ Pressure orifice circumferential location from top vertical centerline of model at zero roll, positive clockwise looking upstream, deg

Configuration Designation

The model configuration is designated by a sequence of letters and numbers. The various groups indicate specific components of the configuration and are defined below.

B1 Force model booster section

B2 Pressure model booster section

P1 Force model payload nose section

P2 Pressure model payload nose section

R1 Force model booster raceway

S1 No seal between nose and booster section (open gap)

S3 Hard metal-to-metal seal between nose and booster sections

T2 Forward boundary-layer trip device

T3 Forward and aft boundary-layer trip devices (see Fig. 3)